



Spatiotemporal characteristics of meteorological drought variability and trends (1981–2020) over South Asia and the associated large-scale circulation patterns

Irfan Ullah^{1,2} · Xieyao Ma^{3,4} · Jun Yin^{3,4} · Abubaker Omer³ · Birhanu Asmerom Habtemicheal^{5,6} · Farhan Saleem^{7,8} · Vedaste Iyakaremye^{9,12} · Sidra Syed¹⁰ · Muhammad Arshad^{11,12} · Mengyang Liu^{4,12}

Received: 4 December 2021 / Accepted: 21 July 2022 / Published online: 11 August 2022
© The Author(s), under exclusive licence to Springer-Verlag GmbH Germany, part of Springer Nature 2022

Abstract

The present study uses observation-based gridded air temperature and precipitation datasets to investigate the spatiotemporal changes in meteorological drought from 1981 to 2020 in South Asia (SA). The drought characteristics i.e., duration, area, frequency, intensity, and severity are calculated using Run theory and the Standardized Precipitation Evapotranspiration Index (SPEI) on annual and seasonal timescales. SA is divided into four homogeneous subregions using the k-means clustering algorithm, while the trends were estimated using Sen's Slope estimator and modified Mann-Kendall (MMK) test. A state-of-the-art Bayesian Dynamic Linear (BDL) model was employed to assess the sub-regional drought variability and their possible links with large-scale atmospheric drivers such as the Indian Ocean Dipole (IOD), El Niño Southern Oscillation (ENSO), and the Pacific Decadal Oscillation (PDO). It is found that the SA winter season experienced a significant drying long-term trend, especially southwestern and northeastern parts of SA. Drought durations show dipolar patterns with longer drought duration in the southwestern compared to the northern parts of SA. Notably, arid and semi-arid regions have shown significant drying trends in terms of their area, frequency, and severity, implying that meteorological droughts are relatively more severe in those regions. Similarly, the relationship varies over time between drought variability and climate drivers. In particular, the IOD has an impact on drought episodes over southwest SA relative to the northern parts and is mostly affected by the Sea surface temperature (SST) variability. The study results contribute to a better understanding of the meteorological drought characteristics over SA, which is important for disaster risk managers and policymakers to mitigate drought impacts.

Keywords Drought · Bayesian model · Climate change · Large-scale drivers · IOD · South Asia

✉ Xieyao Ma
xyma@nuist.edu.cn

¹ College of Hydrology and Water Resources, Hohai University, 210098 Nanjing, China

² CMA-HHU Joint Laboratory for Hydrometeorological Studies, Hohai University, 210098 Nanjing, China

³ School of Hydrology and Water Resources, Nanjing University of Information Science and Technology, 210044 Nanjing, China

⁴ Key Laboratory of Hydrometeorological Disaster Mechanism and Warning of Ministry of Water Resources, Nanjing University of Information Science and Technology, 210044 Nanjing, China

⁵ Collaborative Innovation Centre on Forecast and Evaluation of Meteorological Disasters, Key Laboratory of Aerosol-Cloud-Precipitation of China Meteorological administration,

School of Atmospheric Physics, Nanjing University of Information Science and Technology, 210044 Nanjing, China

⁶ Department of Physics, Wollo University, 1145, Dessie, Ethiopia

⁷ International Center for Climate and Environment Sciences, Institute of Atmospheric Physics, Chinese Academy of Sciences, 100029 Beijing, China

⁸ College of Earth and Planetary Sciences, University of Chinese Academy of Sciences, 100049 Beijing, China

⁹ Rwanda Meteorology Agency, 898, Kigali, Rwanda

¹⁰ Institute of Peace and Conflicts Studies, University of Peshawar, 25000 Peshawar, Pakistan

¹¹ Pakistan Meteorological Department, Sector H-8/2, 44000, Islamabad, Pakistan

¹² School of Atmospheric Science, Nanjing University of Information Science and Technology, 210044 Nanjing, China

1 Introduction

Drought is a recurrent natural hazard with more detrimental effects, affecting a wide range of socio-economic and environmental sectors around the world (Wilhite et al. 2007; Mishra and Singh 2010; Dai 2011; Guo et al. 2018; Huang et al. 2019). Generally, this phenomenon is manifested by prolonged dry spells in nature because of the below-average rainfall and other thermodynamic factors (Vicente-Serrano et al. 2010; Aadhar and Mishra 2020). The start and end of drought hazards is difficult to predict because of various dynamic and thermodynamic mechanisms. In recent decades, global warming-induced drought episodes were already evident in some regions, for instance, the East Africa drought in 2010–2011 (Dai 2011), the United States drought in 2012 (Hoerling et al. 2014), the California drought in 2011–2014 (Seager et al. 2015), the India drought in 2000 (Mishra and Singh 2010), the Pakistan drought in 2000–2004 (Ahmed et al. 2019b), and south-western China drought during 2009–2011 (Yao et al. 2020). The observed changes in meteorological droughts and their relationship with climate variability over South Asia (SA) received less attention notwithstanding the importance of projected changes in water availability. However, it remains unclear how the extreme meteorological drought events in the observed climate that affected surface and groundwater resources, agricultural production, and economic growth in the region will change under the warming climate over SA. Thus, it is important to study and identify the long-term change in droughts and the physical mechanisms associated with droughts in the region.

Several indices have been used globally to monitor droughts (i.e., agriculture, meteorological, and hydrological), which provide actionable information on drought risk assessments and mitigation (Huang et al. 2019; Gu et al. 2020a; Guo et al. 2018; Aadhar and Mishra 2020). These indices include the standardized precipitation index (SPI) (McKee et al. 1993), the Standardized Runoff Index (SRI) (Shukla and Wood, 2008), the Standardized Soil Moisture Index (SSI) (Hao and AghaKouchak 2013), the Palmer Drought Severity Index (PDSI) (Palmer, 1965), and the Standardized Precipitation Evapotranspiration Index (SPEI) (Vicente-Serrano et al., 2010). SPEI has been widely used for drought forecasting and characterization on the regional and global scales (Diaz et al. 2020; Gebremeskel Haile et al. 2020; Gu et al. 2020a; Uwimbabazi et al. 2022).

SA is a drought-prone region due to the complex topography and climate. This region is highly depend on irrigated agriculture (Ali et al. 2019). Most countries in SA (i.e., Afghanistan, Pakistan, India, Nepal, Maldives, Bangladesh, Bhutan, and Sri Lanka) are characterized by arid and semi-arid climate conditions (Adnan et al. 2016; Aadhar

and Mishra 2020; Sajjad et al. 2022). The water resources in the SA region are highly under pressure because of an increase in water demand with significant population growth (Shahzaman et al. 2021b; Xing et al. 2022; Ullah et al. 2022a). A substantial rise in temperature and small or/ no change in precipitation is evident over SA during the last few decades (Ali et al. 2019; Jiang et al. 2020; Almazroui et al. 2020; Iyakaremye et al. 2022; Lu et al. 2022). On the other hand, uncontrolled human-induced activities could also trigger drought occurrences. For instance, the Arabian Sea's dryness has significantly influenced the local climate, with more than 2-times drought occurrences over the SA domain (Aadhar and Mishra 2020). In recent years, due to an increase in drought risks, the research on drought in SA has received enormous attention. For example, Aadhar and Mishra (2020) studied the increased drought risk using different approaches of potential evapotranspiration (PET) under a warming climate in SA during 1979–2018. Ali et al. (2019) investigated the response of vegetation dynamic to seasonal drought over SA (1990–2011), while Zhai et al. (2020) studied the future drought variation using a multi-model ensemble based on SPEI and PDSI in the SA and found a drying trend in the last few decades. Considering the differences in drought trend, evolution, and spatiotemporal characteristics, it is important to study the drought behaviors in distinct regions. Though various studies focused on meteorological drought in SA, less attention was paid to the drought features at the sub-regional scales. Thus, to better understand the drought evolution and its features (i.e., drought onset, magnitude, area, and severity), it is essential to identify the drought prone areas in order to develop a proper future drought mitigation and adaptation strategies.

This research mainly provides a comprehensive assessment of the spatial and temporal variability of droughts using SPEI over SA and its subregions. Precisely, the objectives of this study are (1) to check the annual and seasonal drought trends based on the modified Mann-Kendall and Sen's Slope estimator; (2) to delineate the possible association between seven large-scale climate drivers and drought variability in SA and its subregions using state-of-the-art Bayesian Dynamic Linear (BDL) model. The present study's findings would provide actionable information to the scientific community and the public for disaster risk reduction in SA and its subregions. The rest of the paper is organized as follows: Sect. 2 provides the details about the study area, datasets, and opted methodologies; the study results are given in Sect. 3, while Sects. 4 and 5 present discussion and conclusions.

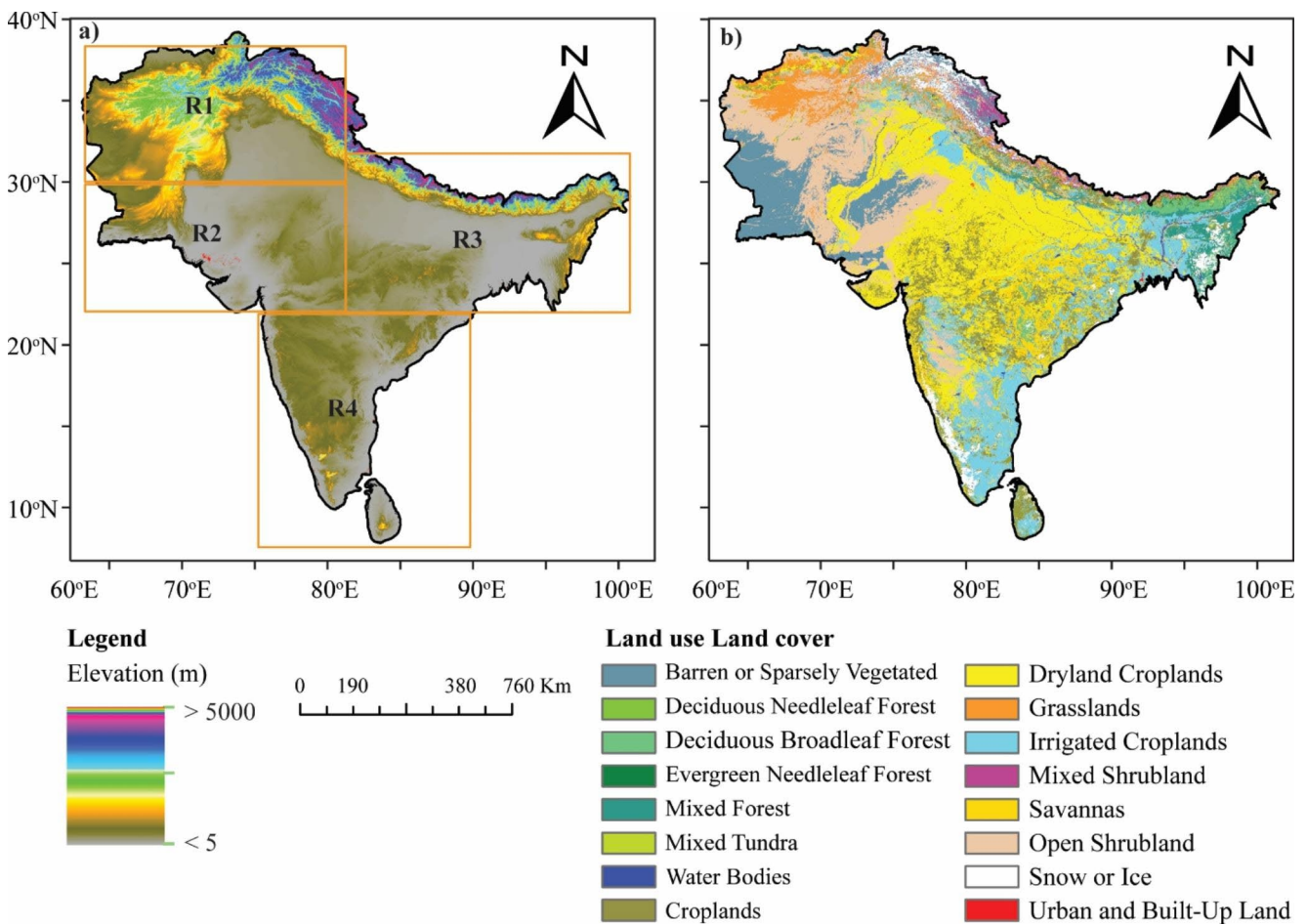


Fig. 1 Study area and target subregions (i.e., Region-1, Region-2, Region-3, and Region-4 are represented with R1, R2, R3, and R4, hereon) of the current study presented with light orange boxes in Fig. 1a, along with elevation and land use/cover changes shown in Fig. 1b

2 Data, Study Area, and methods

2.1 Study area

The study domain comprises eight countries (i.e., Afghanistan, Pakistan, India, Nepal, Maldives, Bangladesh, Bhutan, and Sri Lanka) located in SA (Fig. 1). The topography of SA consists of high mountains in the north, for instance, the Hindu-Kush Himalayan range, the Indian Ocean in the south, the Indus and the Ganges River basins in the western parts (Aadhar and Mishra 2020). The elevation ranges from 0 m in the coastal and lowlands regions to more than 8000 m in the Himalayan region. Due to SA's diverse landscape and geographical location, the region is categorized into arid and semi-arid climates with low relative humidity (Ahmed et al. 2019b; Ali et al. 2019; Mishra et al. 2020). Moreover, due to the influence of climate change and human-induced activities (Guo et al. 2018; Xu et al. 2020), water scarcity in SA is getting worse. Thus, the region is considered one of the driest regions in the world. However, the SA has four distinct climatic zones, including subtropical (e.g., northwest

India, highlands in Pakistan, and Afghanistan), tropical (e.g., south India and southwest Sri Lanka), semi-arid (e.g., central parts of SA), and arid (e.g., Northern India, south Pakistan, and large parts of Afghanistan) (Mohsenipour et al. 2018; Gaire et al. 2019; Khatiwada and Pandey 2019; Arshad et al. 2021a). Recently, Ullah et al. (2022b) investigated the anticipated changes in socioeconomic exposure to heat waves in SA and its four distinct subregions under changing climate. They found that most SA regions have experienced heat stress events with a larger geographical extent and are anticipated to become more severe by the end of the 21st century. Thus, we examine the impact of different climate variability on the evolution, severity, and magnitude of observed droughts across the four subregions that have distinct precipitation seasonality and cover key breadbaskets and highly vulnerable population.

2.2 Datasets

One of the key issues in investigating hydro-climatological events is the lack of available long-term records and reliable

climatic observation around the globe (Ahmed et al. 2018; Arshad et al. 2021b; Ullah et al. 2022b). To overcome these problems, an effort has been made to develop several multi-source climate products, i.e., gauge-based, satellite-based, and reanalysis products. Among those, gauge-based gridded datasets are frequently used due to their robust spatiotemporal continuity and accessibility over a longer time (Kishore et al. 2016). Besides, the gauge-based gridded datasets have better spatial performance and continuous availability than the traditional gauge observations, which play a vital role in describing drought characteristics (Guo et al. 2018; Ahmed et al. 2018; Yang et al. 2020).

This study uses the latest version of Climatic Research Unit Version 4.05 (CRU TS4.05) of monthly mean, maximum, and minimum air temperature datasets from 1981 to 2020. The CRU TS4.05 dataset was developed by the University of East Anglia and can be found online through (<http://www.cru.uea.ac.uk/data/>). In addition, this study also used the monthly precipitation obtained from the Climate Hazard Group Infrared Precipitation with Station Data (CHIRPS), which can be found online at <https://data.chc.ucsb.edu/products/CHIRPS-2.0/>, from 1981 to 2020. CHIRPS is a combined product of remotely sensed and in-situ observations developed for monitoring droughts and climate extremes. At the start, CHIRPS was designed to support the United States Agency for International Development Famine Early Warning Systems Network (FEWS-NET). It followed the effective procedures used in generating the Thermal Infrared (TIR) precipitation products like the National Oceanic and Atmospheric Administration's (NOAA's) Rainfall Estimate (RFE2) and African Rainfall Climatology. The selection of CRU TS4.05 and CHIRPS datasets to calculate the SPEI index is based on many reasons. First, they comprise high station density and have undergone strict quality control and time uniformity test (Wang et al. 2014). Second, they have a high spatial resolution ($0.5^{\circ} \times 0.5^{\circ}$) with 5600 grid-points covering SA and long-term records suitable for drought assessment (Guo et al. 2018). Recently, numerous studies utilized CRU TS and CHIRPS datasets to estimate SPI and SPEI to study various meteorological-related research and obtained promising results in Asia (Ahmed et al. 2019a; Jiang et al. 2021; Shahzaman et al. 2021b). Therefore, to better understand the historical drought occurrences over SA and its subregions, we select the data from 1981 to 2020 (40 years).

The climate of SA is influenced mainly by three factors: the Pacific Decadal Oscillation (PDO), the Indian Ocean Dipole (IOD), and the Dipole Mode Index (DMI) (Guo et al. 2018; Kang and Lee 2019; Shah and Mishra 2020a). It has been found that the multivariate El Niño Southern Oscillation (ENSO) has a close association with the occurrence of drought in SA (Liu et al. 2015; Joshi and Kar 2018; Gaire et

al. 2019). Therefore, IOD, PDO, DMI, ENSO, Sea Surface Temperature (SST), Central Tropical Pacific SST (Niño3.4), and solar activity represented by Sunspots are considered to study the interconnection between drought variability and large-scale climate patterns. The Niño3.4 index is used to define ENSO as the average SST anomalies over 5°S – 5°N , 170° – 120°W region. We also calculate the fraction of the total drought events in each region during different phases of these modes of oceanic variability. Therefore, the present study checks these modes as individual factors to better understand the oceanic and atmospheric variability of drought events.

The present study uses IOD and DMI indices calculated as the SST difference between the western (50° – 70°E , 10°S – 10°N) and eastern (90° – 110°E , 10°S –Equator) the equatorial Indian Ocean. An SST dipole between the western and eastern tropical Indian Ocean, while the Intensity of the IOD is presented by anomalous SST gradients between the western and the southeastern equatorial Indian Ocean. Therefore, individual use of IOD and DMI was a prime target to understand the dynamic factor solely, as SA is surrounded by the Arabian Sea, Indian Ocean, and the Bay of Bengal. On the other hand, the major driver of monsoonal climate systems is the sunspot, and other particular features including land-sea circulation pattern, topography, and ocean movement. These drivers are mostly responsible for precipitation concentration and intensity variation in a specific region. It should be noted that the inter-annual variation of the monsoonal climate may also come from thermodynamic feedback systems. The feedback systems such as multivariate ENSO and IOD could cause changing behaviors of precipitation based on inter-annual timescales over various regions including SA. Change in precipitation concentration and intensity behaviors in SA has a strong relationship with the Sunspot, which moved southward due to enhance west-lies, and precipitation cycles may be affected by their second-largest influence on the South Asian Summer Monsoon. Thus, monthly datasets (1981–2020) for each climate index were obtained from (<https://psl.noaa.gov/data/climateindices/list/>). The detailed information of the seven indices is shown in Table S1.

2.3 Methods

2.3.1 k-means algorithm

SA has complex climatic regimes where spatial variability of the precipitation and temperature changes as a function of the major circulation patterns (Ali et al. 2019; Preethi et al. 2019; Aadhar and Mishra 2019). These regions are also affected by other factors, for instance, landscape, topography, coastal vicinity, or latitude (Khan et al. 2020; Shah and

Mishra 2020a). A k-means clustering method was applied to the 3-month SPEI (Guo et al. 2018; Yang et al. 2020) to analyze the drought occurrence over the different homogenous subregions and its association with large-scale climate drivers. The k-means algorithm can produce different clusters with the aim of; (1) minimizing variability with the number of clusters k , and (2) maximizing variability of each centroid among all the data series. The k-means algorithm provides a better partition result when a large number of grids (more than 5600 points) are considered. Liu et al. (2018) applied the Silhouette index over southwest China to investigate the long-term change of PET using k-means clustering during 1961–2013 and divided southwest China into four subregions. To explore the multi-model spatiotemporal mesoscale drought projections in India, Gupta and Jain (2018) applied a k-means clustering algorithm to the SPEI and SPI time series and divide India into six clusters. Thus, the present study uses k-means clustering and divides SA into four different subregions that include region-1 (R1), region-2 (R2), region-3 (R3), and region-4 (R4), respectively.

2.3.2 The Standardized Precipitation Evapotranspiration Index (SPEI)

The SPEI (Vicente-Serrano et al. 2010) is a robust index for drought monitoring and analysis in the context of climate change at global and regional scales (Wang et al. 2014; Guo et al. 2018; Mohsenipour et al. 2018; Ahmed et al. 2018). Therefore, based on several advantages, SPEI was applied as a drought index in this study. SPEI considers a simple climatic water balance with the difference between precipitation and PET. Besides, SPEI indicates precipitation shortages and reveals water scarcity caused by excessive evapotranspiration. Therefore, it is found to be more effective in detecting the temporal variability of droughts in a diverse regions (Frank et al. 2017). Wang et al. (2014) investigated the changing characteristics of severe droughts on a global scale during 1902–2008 based on the SPEI index and found an increasing trend in drought areas worldwide. For further details about SPEI, readers are suggested to Vicente-Serrano et al. (2010). In addition, the SPEI value between -1.0 to -1.5 is considered moderate drought, the value between -1.5 to -2.0 demonstrates severe drought, and below -2.0 values represent extreme severe drought.

There are many approaches to calculate PET, however, Thornthwaite (1948) (TH) and Penman-Monteith (PM) (Allen et al. 1994) are the two most widely used methods. Since the TH equation is only based on temperature, PET intends to be underestimated in the arid and semi-arid areas (Vangelis et al. 2013). Based on the physical calculation process, the PM is considered one of the most accurate approaches to calculate PET (Guo et al. 2018). The

superiority of PM over TH in the calculation of SPEI has been verified in previous studies (Mishra and Singh 2010; Guo et al. 2018; Khan et al. 2020). Therefore, considering the arid and semi-arid climate in SA, we prefer to use PM-based SPEI as the drought index in this study.

In this study, 3-month SPEI for a given month is calculated based on the present month and the prior two months; for instance, February indicates the Dec-Jan-Feb precipitation and PET of the 3-month SPEI index. Therefore, we used the 3-month SPEI values for February, May, August, and November for seasonal analysis for winter, spring, summer, and autumn, respectively. On the other hand, the 12-month SPEI values for December were adopted as the annual timescale for analysis.

2.3.3 Drought trend detection

The nonparametric Mann-Kendall (MK) trend test is one of the most commonly used hydro-meteorological time series approach to detect trends/changes in auto-correlated SPEI data (Mann 1945; Bevan and Kendall 1971). The test does not require normal distribution and is effective against outliers, missing values, and abrupt changes in time series. The existence of autocorrelation in the data could probably affect the trend detection. Therefore, Hamed and Rao (1998) recommended a trend estimator to subtract from the original time series while evaluating the autocorrelation. The modified-MK test was then applied to the SPEI time series, and the trends with p -values < 0.05 were considered statistically significant. We used the nonparametric Sen's Slope estimator to evaluate the trend magnitude (Sen, 1968), while the Pettitt test (Pettitt, 1979) was also applied to detect the abrupt change points.

2.3.4 Drought event identification and characterization

The Run theory, proposed by Yevjevich (1967), which is one of the most frequently used approaches for identifying drought parameters, was adopted in this study. A run is defined as a portion of the time series of a variable in which all values are less or greater than the selected threshold value; therefore, the runs can be either a negative or a positive (Guo et al. 2018; Yang et al. 2020). This definition has two main reasons; firstly, the consistent low drought intensity could also greatly influence vegetation growth, agricultural production, and the environment (Sheffield et al. 2012; Wang et al. 2014). Secondly, identifying drought events starting from negative SPEI values can help improve the early warning system. Once the drought event is defined, it can be referred to as drought duration (Dd), drought frequency (Df), drought severity (Ds), and drought peak (Dp) using the Run theory. Dd is the number of months between

the drought onset time and the termination time. D_s is the cumulative sum of SPEI values during a drought event, while D_f is the number of drought events that occurred during the considered period. Details of the variables describing drought events are given in (Mishra and Singh, 2010; Guo et al. 2018).

2.3.5 Multivariate return period with most likely realization approach

In literature, various studies usually examined the changes in drought duration or severity under a warming climate independently, neglecting the multiplex behavior of droughts (Gu et al. 2020b). This study provides D_d and D_s jointly via the copula function, which is multipurpose for describing dependent hydro-meteorological variables due to its flexible marginal distributions. The widely used Gamma distribution was adapted to fit the drought variables in grid points over the SA, and we selected the Gumbel copula to attain the joint distribution of D_d and D_s . Different definitions of joint return periods have been developed in copula-based methods, such as the OR, AND, Kendall, dynamic, and structure-based return periods (Guo et al. 2019). Amongst these, the OR case (T_{or}) is generally used in drought occurrence assessment (Zhao et al. 2020):

$$T_{or} = \frac{E_l}{1 - F(d, s)} = \frac{E_l}{1 - C[F_D(d), F_S(s)]}, \quad (1)$$

where E_l indicates the expected time interval of drought events, $F_D(d)$ and $F_S(s)$ represents the marginal distribution functions of duration and severity, while the joint distribution $F(d, s)$ could be defined based on copula function $C[F_D(d), F_S(s)]$, respectively.

Based on the multivariate framework, the optimal choice of T_{or} leads to unlimited combinations of D_d and D_s . The drought events, along with the T_{or} -level curve is usually not equal concerning societal and environmental consequences; however, the probability of each event must be prioritized when considering appropriate joint quantiles. The most likely realization approach is adopted in this paper, selecting the drought condition with the highest probability along with T_{or} -level curve (Yin et al. 2019), which can be derived as:

$$\left\{ (d^*, s^*) = \underset{C(F_D(d), F_S(s)) = 1 - E_l/T_{or}}{\operatorname{argmax}} f(d, s) = c[F_D(d), F_S(s)] f_D(d) f_S(s) \right\}, \quad (2)$$

in Eq. 2, $f(d, s)$ denote the joint probability density function, where $C(F_D(d), F_S(s)) = c[F_D(d), F_S(s)] f_D(d) f_S(s)$ represents the density function of the copula, while $f_D(d)$

and $f_S(s)$ are the likelihood density functions of drought duration (d) and severity (s), respectively.

2.3.6 Bayesian dynamic linear model

To evaluate the time-varying impacts of large-scale climate dynamics on droughts, we applied a state-of-the-art Bayesian dynamic linear (BDL) model from 1981 to 2020. Unlike the versatile linear regression, which has stationary coefficients regression, the BDL model had the strength of dynamic and time-varying association between climate drivers and drought. Therefore, it has higher accuracy than the traditional linear regression (Yang et al. 2020). BDL model has been widely used to identify the time-varying features of time series in hydrometeorology and climate research. For example, Yang et al. (2020) used the BDL model for the dynamical influences of large-scale potential climate drivers on droughts over four different subregions in Canada. Another study by Gao et al. (2017) used BDL to investigate the dynamic impact of IOD, ENSO, PDO, North Atlantic Oscillation (NAO), and Atlantic Multi-decadal Oscillation (AMO) over extreme regional precipitation of China during 1960–2014. However, none of the studies used the BDL model over SA, even though very few studies have used the BDL model for droughts analysis. The mathematical equation for the BDL model can be described as follows (Gao et al. 2017; Yang et al. 2020):

$$\begin{cases} y_t = a_t + x_t \beta_t + v_t, & v_t \sim N(0, V_t) \\ \alpha_t = \alpha_{t-1} + \omega_{\alpha,t}, & \omega_{\alpha,t} \sim N(0, \omega_{\alpha,t}) \\ \beta_t = \beta_{t-1} + \omega_{\beta,t}, & \omega_{\beta,t} \sim N(0, \omega_{\beta,t}) \end{cases} \quad (3)$$

where y_t indicate response variable for drought index, x_t is the covariate in terms of climate pattern, while α_t and β_t represents the dynamic intercept and slope coefficient at time t , respectively, whereas the error sequences V_t , $\omega_{\alpha,t}$, and $\omega_{\beta,t}$ are independent, both within them and between them.

3 Results

3.1 Homogenous subregions

The South Asian region exhibit a clear spatial variability in rainfall and temperature due to various climatic regimes and complex landscape. Therefore, it is essential to analyse drought considering homogeneous regions. Figure 2 indicates the annual mean SPEI series for the four subregions of SA. Amongst them, R1, R2, and R4 depict a significant increasing trend during 1981–2020, implying that droughts

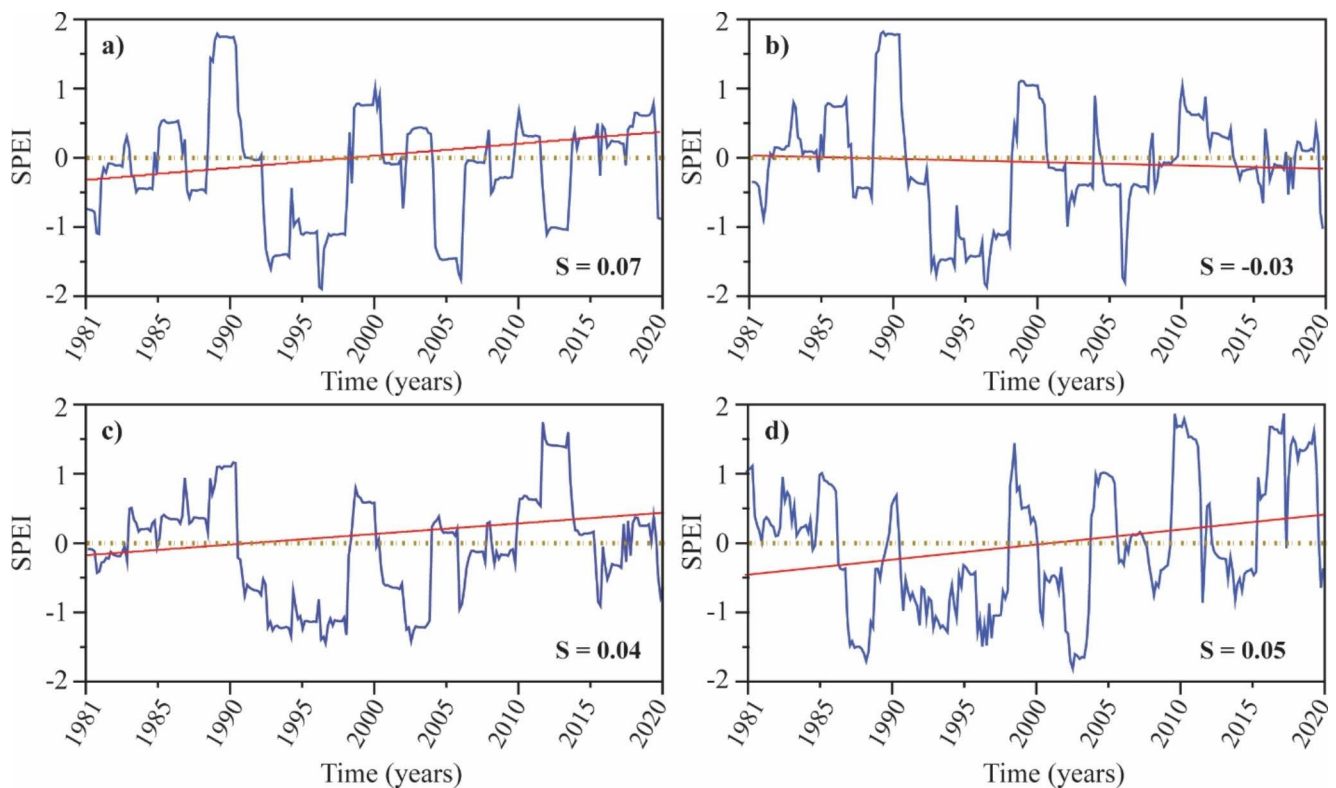


Fig. 2 Annual SPEI time series for four SA target subregions, namely R1 (a), R2 (b), R3 (c), and R4 (d), respectively. The red line indicates a linear trend and S is the trend using Sen's slope. Note that S values shown at the bottom-right of each panel are statistically significant at the 95% confidence interval using the modified-MK test

in the south-central and western SA experienced relatively more severe drought in recent decades.

Almazroui et al. (2020) recently studied the projections of precipitation and temperature over the SA regions and found a significant rise in annual mean temperature. A robust increase was revealed in winter precipitation over the western corresponding to the eastern Himalayas. They also found that the mean annual temperature is projected to increase by the end of the 21st century, particularly in the arid region of southern Pakistan and adjacent areas of India, corresponding to R2 and R4 considered in this study. To investigate the seasonal variability of precipitation and temperature of Aadhar and Mishra (2019) found a higher increase in the seasonal monsoon precipitation due to their higher sensitivity of convective precipitation to warming. They also showed that the risk of dryness and water scarcity is highly under a warming climate over SA than previously reported. This could be possibly due to the variations in large-scale atmospheric circulations significantly affecting a larger area than a single climate or ecological region.

3.2 Trend in seasonal drought

Figure 3 indicates the spatial pattern of the modified-MK trend statistic of the seasonal SPEI over SA subregions

during 1981–2020. The results reveal complex spatial variations in distinct seasons; however, significant positive trends dominated over whole SA while negative trends during the autumn season are not statistically significant, which further clarifies our results in Fig. 2. In spring, stiff significant increasing trends are predominantly exhibited over the northern Himalayas of R1. During summer, R1, R2, and R4 show more significant increasing trends than in the spring season. Moreover, southern Pakistan and eastern Afghanistan (R1) have revealed relatively weaker negative trends in summer than in spring. Furthermore, the higher significant decreasing trends are observed in the south-eastern parts. In autumn, a similar pattern can be seen as that for spring, except for southern R1, central-east R2, and whole parts of R4, while winter exhibit increasing trends mainly over northern Pakistan and north and south India, respectively (Fig. 3d). In northern foothills mountainous regions and south-central of SA, a prevalent decreasing trend appear, suggesting that winter has an obvious drying tendency among the four seasons (see Fig. S1).

According to Sheikh et al. (2015), variations in the frequency of temperature extremes are obvious over SA with warm extremes becoming more frequent than the cold extremes. They also found that extreme precipitation indices exhibit mixed behavior than temperature (Aadhar and

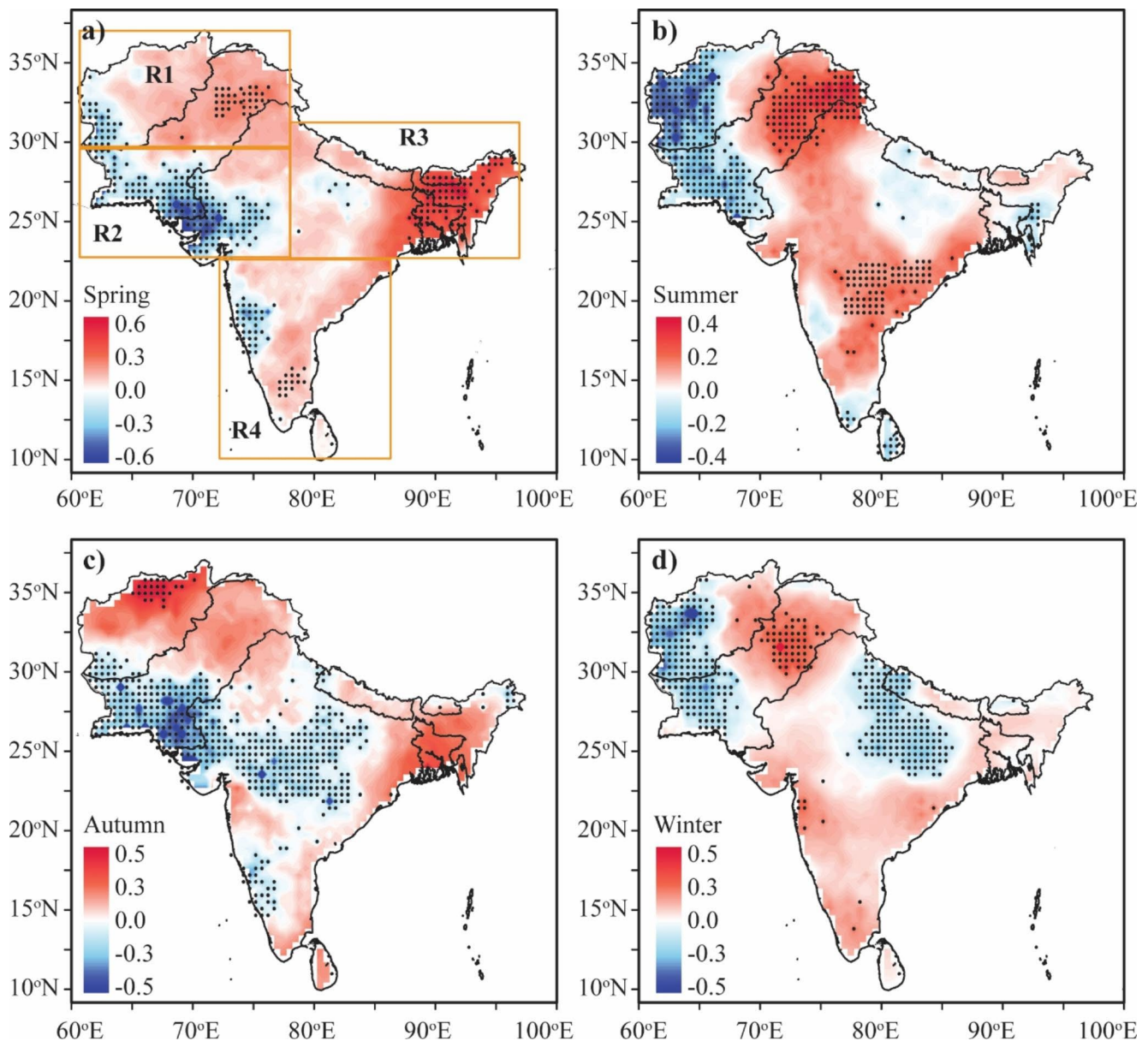


Fig. 3 Spatial distributions of the secular modified-MK trend statistic for the seasonal 3-months SPEI over the four subregions of SA i.e., spring (a), summer (b), Autumn (c), and winter (d). The black dotted circles represent the significant positive and negative trend at a 95% significant level, while the light orange boxes represent study subregions

Mishra 2020), whereas relatively small scales spatially coherent changes are evident. Furthermore, south and western SA experienced a warming pattern (Rehman et al. 2018; Almazroui et al. 2020), while cooling in the northern is evident during the winter and spring seasons (Liu et al. 2015). These all together could have attributed to the tendency of drying trends detected in south-western SA (winter) and wetter trends in northern Himalayan (spring). Using the UNESCO aridity index, Ahmed et al. (2019) indicated that the spatial pattern of aridity trends exhibits strong precipitation changes in the aridity trend over Pakistan. They also stated that the climate of southern Pakistan has more than

60% arid. Qutbudin et al. (2019) reported that temperature is the major factor influencing the decreasing trend in the seasonal SPEI values across Afghanistan, which increased up to 0.14°C/decades. Similarly, Preethi et al. (2019) analyzed the Indian summer monsoon drought variability over SA, including India and found a significant increasing trend in monsoon rainfall, which agree with the findings in Fig. 3d. Based on previous studies, it can be inferred that our findings further clarified that the drought risk in the winter season has worsened.

3.3 Observed changes in drought characteristics

3.3.1 Spatiotemporal changes in drought severity and frequency

Changes in drought severity and frequency over SA and its subregions were assessed from 1981 to 2020 (see Fig. 4). The absolute value of $\text{SPEI} \leq -1$ is multiplied by duration to define the total drought severity (TDS), and the results are presented in Fig. 4A. The result indicated that all subregions exhibit relatively decreased drought severity. At the same time, R4 showed increasing drought severity, demonstrating that the severity of drought events has gradually reduced in most regions except R4. Moreover, most of the regions suffered from severe droughts, especially for R4. Our results concur with the findings of previous work (Gaire et al. 2019; Shah and Mishra 2020b). They found that east and western India, under dry conditions, experienced severe drought and are expected in the near future, which further justifies results in R3 and R4. Another possible reason could be the Indian Ocean generating increased precipitation activity during the positive phase of the IOD event, reinforcing the equatorial flow to the Bay of Bengal caused by the strong meridional SST gradients across SA (Ummenhofer et al. 2013; Pathak et al. 2017; Lu et al. 2018; Preethi et al. 2019; Aadhar and Mishra 2020).

The severe and extreme drought severity (SEDS) were evaluated at annual $\text{SPEI} (\leq -1.5)$ for four homogeneous regions (Fig. 4a and d). The annual SEDS in all areas has decreased at the rate of $-0.3/\text{decade}$, $-0.2/\text{decade}$, and $-0.5/\text{decade}$ over R1, R2, and R3, respectively, except R4 ($0.1/\text{decade}$) (Table S2), which further clarify the spatial results (Fig. 4A). Although the SEDS trend shows positive after the 2000s for R1 and R4, the magnitude was relatively small compared to the negative trend from 1980 to 2010 s, implying that the 2000s was a worsened decade influenced by intensified and prolonged droughts in the region. It can be inferred that the usual decrease in SEDS is significantly attributed to the general decline of TDS across SA from 2000 to 2010 (Fig. S3). The results above concurred with previous drought studies (Mishra et al. 2017; Almazroui et al. 2020). For instance, using SPEI based on five PET estimations, Aadhar and Mishra (2020) indicated a significant warming climate in the south and western SA during 1980–2018. Likewise, under a warming climate, the summer monsoon could cause heavy precipitation at high-northern latitudes (Latif et al. 2018), possibly leading to wet conditions over the foothills Himalayans.

The spatial distribution of total drought frequency (TDF) on annual $\text{SPEI} (\leq -1)$ over SA subregions is presented in Fig. 4B. Overall, the south and northern SA appeared with more severe drought events covering R1 and R2; however,

a slight increase can be seen in R3 than R4. Similar results were obtained by Ahmed et al. (2018) and Qutbudin et al. (2019); they found that drought frequency and severity are increasing over predominantly arid and semi-arid regions of southern Pakistan and northern Afghanistan. Moreover, R1 and R2 are located in the westerly and monsoon core regions, which are highly affected due to long-term temperature change (Adnan et al. 2016; Latif et al. 2018; Ain et al. 2020).

Unlike the TDF, the annual severe and extreme drought frequency (SEDF) ($\text{SPEI} \leq -1.5$) exhibited a significant decreasing trend for R1 ($-0.4/\text{decade}$), R2 ($-1.0/\text{decade}$), and R3 ($-0.6/\text{decade}$) except for R4 ($0.3/\text{decade}$) detect positive trend (Fig. 4e h). Besides, drought in R4 is less frequent as compared to R1, R2, and R3. According to Gu et al. (2019), they point out that lower frequency usually leads to low adaptability, which makes the region more prone to the impacts of severe drought. For instance, southern Pakistan, Nepal, and the foothills Himalayans are vulnerable to drought due to their high altitude of mountainous ranges with less rainfall and higher spatiotemporal variability.

3.3.2 Spatiotemporal changes in drought duration

The spatial distribution of longest drought duration (LDD) is presented in Fig. 5, which is defined as the longest cumulative months of the $\text{SPEI} \leq -1$ over four subregions of SA during 1981–2020. Results indicated that more than 12-months of LDD is evident over most SA subregions (Fig. 5a). It can be seen from Fig. 5 that LDD shows the dipolar pattern over SA; whereas the western and central SA tends to have longer LDD (10–30 months), while southern and eastern parts exhibit shorter drought duration (2–10 months). Figure 5b shows the spatial pattern of decadal LDD occurring time over homogenous subregions, where R4 (southern SA) appeared relatively stricken due to coherent LDDs since the 1980 and 1990 s. Moreover, the northern (Pakistan), the western (Afghanistan and Pakistan), and north (Nepal and India) have been severely affected in the past few decades (after the 2000s), inferring that north and west SA experienced more prolonged droughts in recent decades (see Fig. S2).

Figure 6 depicts the temporal variations of the annual total drought duration (TDS) for the SA subregions. Results show that R1, R2, and R3 experienced significant increasing trends with the amount of 0.2 month/decade , 0.1 month/decade , and 0.3 month/decade , except R4, which depicts a negative trend $-0.2 \text{ month/decade}$ (Fig. 6a and d), respectively. Also, R1, R2, and R3 evident longer-duration droughts circa after the 2000s; in contrast, R4 captured short-term drought duration during the 2010s. Based on slope change point results (Table S2), the abrupt changes

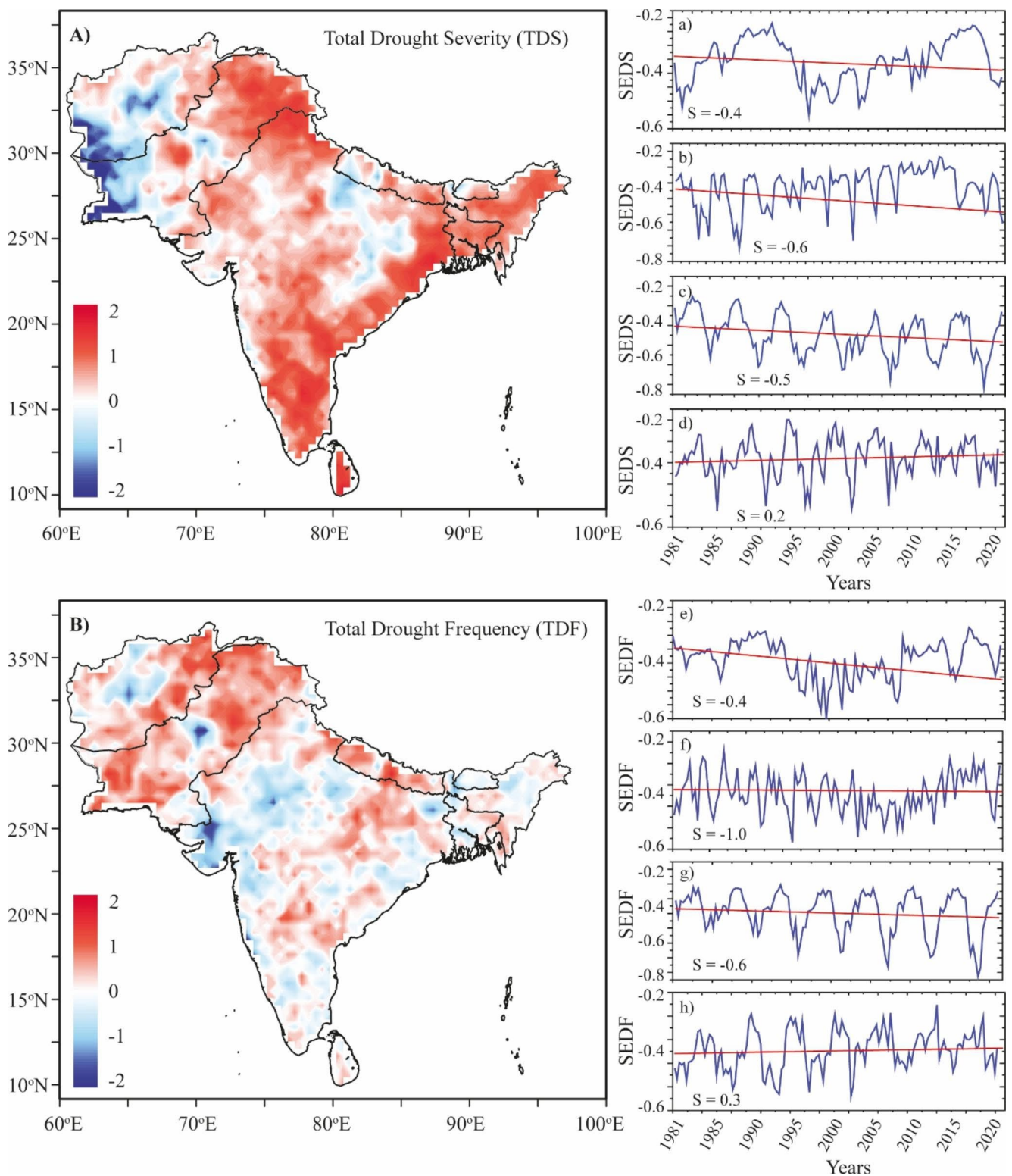


Fig. 4 Spatial and temporal patterns of drought severity and drought frequency over four different climate regions of SA during 1981–2020. Total drought severity (TDS) showed in the left panel (spatial plot A) while severe extreme drought severity (SEDS) was presented in the right panel (temporal plots a, b, c, and d). Similarly, total drought frequency (TDF) is shown in the left panel (spatial plot B), while severe extreme drought frequency (SEDF) is illustrated in the right panel (temporal plots e, f, g, and h). In temporal panels, the red line indicates the linear trend and S is the trend per decade using Sen's slope (S significant values are on the bottom of each panel)

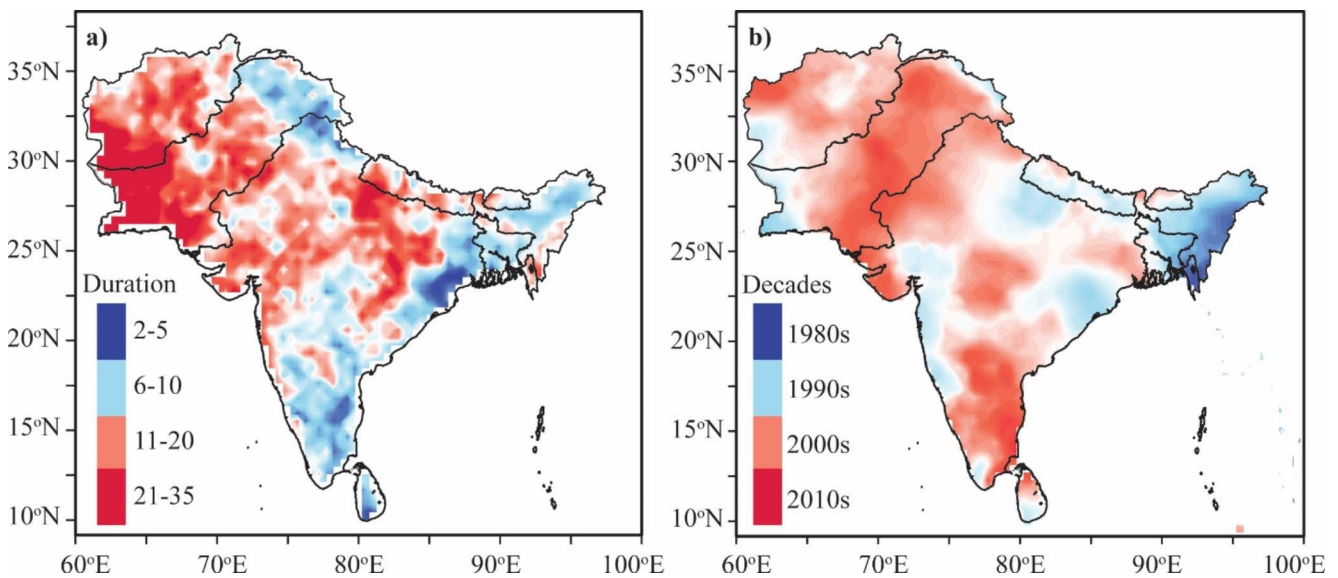


Fig. 5 Spatial distribution of the longest drought duration (a) and the longest drought occurring time (b) over four subregions of SA during the period of 1981–2020

occurred in southern SA in the 2000s, while the rest of the regions show an abrupt change in total drought duration (TDD) in the earlier 2000s.

The temporal evolution of the annual severe and extreme drought duration (SEDD) with SPEI (≤ -1.5) for the four distinct SA regions is shown in Fig. 6e h. The results indicate that overall drought duration reveals complex behavior; however, R1 (-0.3 month/decade) and R2 (-0.4 month/decade) show a significant decreasing tendency, while an increasing trend has been observed in R3 (0.5 month/decade) and R4 (0.4 month/decade) (see Table S2), respectively. Besides, R4 has encountered a higher declining SEDD trend among all four homogenous regions, which may have been caused by the natural variability of regional climate and the rapid drought intensity/frequency shift in climate regime that may occur in the future. Severe and extreme events are obvious in the south and west SA that have significantly contributed to the general decrease of TDD in the region. Notably, between 2000 and 2007, the northeast parts suffered one of the worst and most prolonged droughts in SA history, as well-captured by the SPEI in Fig. 5b. Likewise, the region that appeared with LDD in SA was predominantly located in the western disturbance and monsoon core region, which is in agreement with (Ahmed et al. 2018; Gaire et al. 2019).

3.3.3 Observed changes in the drought area

The temporal evolution of annual total drought area (TDA) variability for four subregions during 1981–2020 is shown in Fig. 7a and d, defined as the percentage of grids with SPEI values less than -1 over the total grid points.

The result indicates that R3 observed a significantly negative trend with the amount of $-5\%/decade$ (Fig. 7c). On the other hand, more widespread TDAs can be seen in R1 and R4 ($30\%/decade$ and $40\%/decade$, respectively), while the lowest and most persistent TDA has appeared in R2 at the rate of $25\%/decade$. In terms of annual timescale, prevalent droughts have followed the whole SA between 2001 and 2005 (see Fig. S2 and S3). Subsequently, worsened droughts occurred in the 2000, 2005, and 2010 for R1 ($>35\%/decade$), in 2002 and 2011 for R2 ($>40\%/decade$), in 2013 and 2017 in R3 ($>60\%/decade$), 2017 and 2018 for R4 ($>65\%/decade$), respectively. The TDA of R4 seems to increase after the 2010s (Fig. 7d), though the magnitude is much smaller than in 1991–2000. In that case, we can say that spatially less widespread drought has occurred over SA after the 1990s.

As for severe and extreme drought areas (SEDA), the annual time series of SPEI ≤ -1.5 were applied over four homogenous subregions of SA (Fig. 7e and f). Overall, SEDAs exhibit complex behavior; however, the abrupt change points shift to R2 detects a decreasing trend with $-4.5\%/decade$ (Fig. 7f) as shown for TDAs in R3 (Fig. 7c). Besides, an abrupt increasing trend has occurred in R1, R3, and R4 with $70\%/decade$, $30\%/decade$, and $50\%/decade$, respectively. A similar pattern can be seen for SEDAs, where abrupt change points are obvious after the 2010s, which has also occurred for TDAs. It can be noted that estimated decreasing trends for TDA and SEDA of R3 ($-5\%/decade$) and R2 ($-4\%/decade$) are seen in Fig. 7c and f, suggesting that the marginal decrease in drought areas in those regions influenced by more mild drought events occurred in recent few decades.

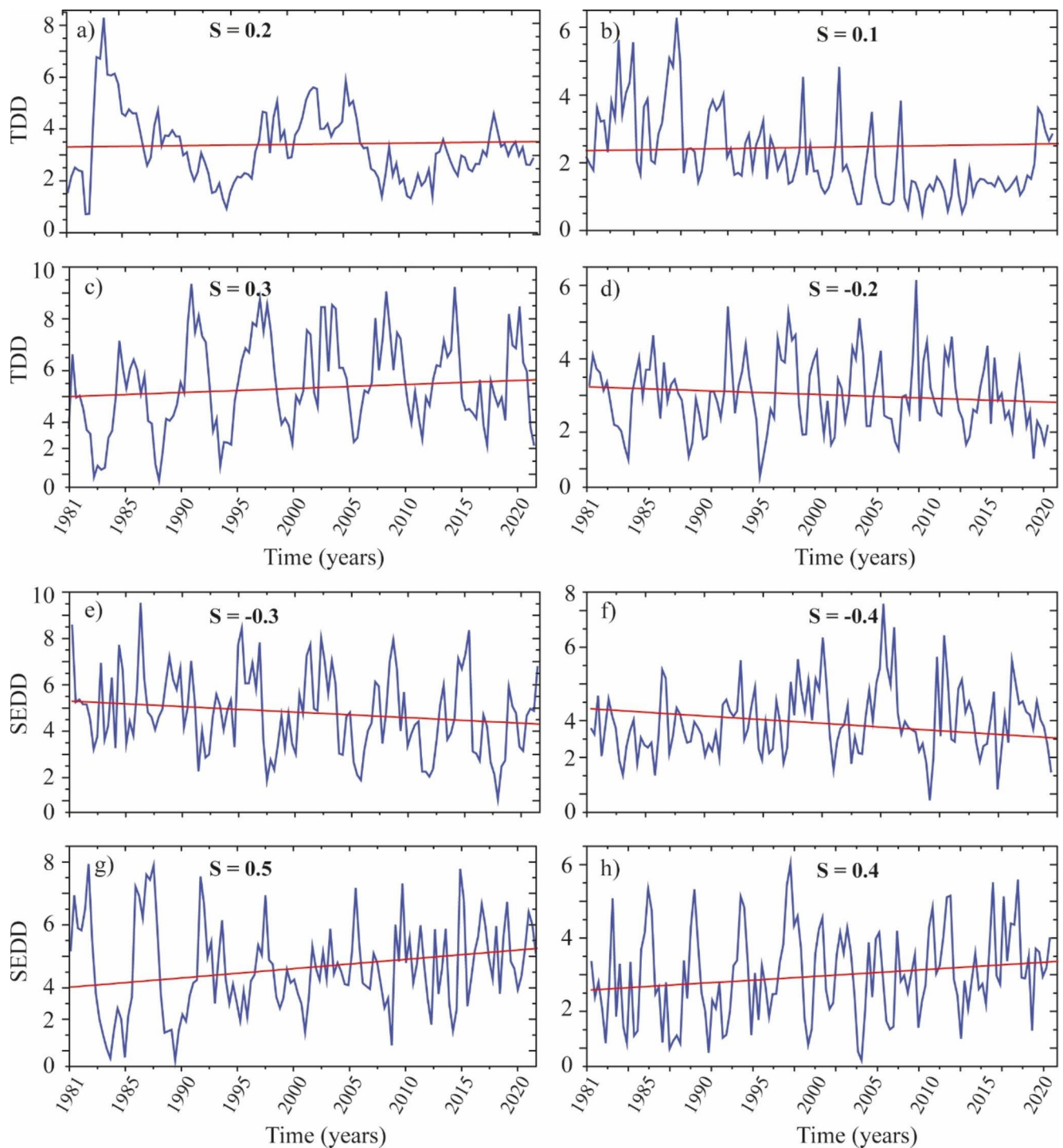


Fig. 6 Temporal variations of annual total drought duration (TDD) (a, b, c, d), and severe extreme drought duration (SEDD) (e, f, g, h) for four distinct climate regions of SA throughout 1981–2020. The red line shows a linear trend while S is the trend per decade using Sen's slope (S significant values are on top of each panel)

It can be inferred from the figure results that overall drought areas have significantly increased in most parts of the SA. However, Ahmed et al. (2018) studied the seasonal drought characteristics during 1901–2010 and found an increased drought area in the 2010s over southern Pakistan,

which further justifies our findings for the 2010s. Recently, Aadhar and Mishra (2019) projected an increase in a drought area, which is highly exposed to increased dryness over SA, emphasizing our findings that have been well-captured by the R1 and R4.

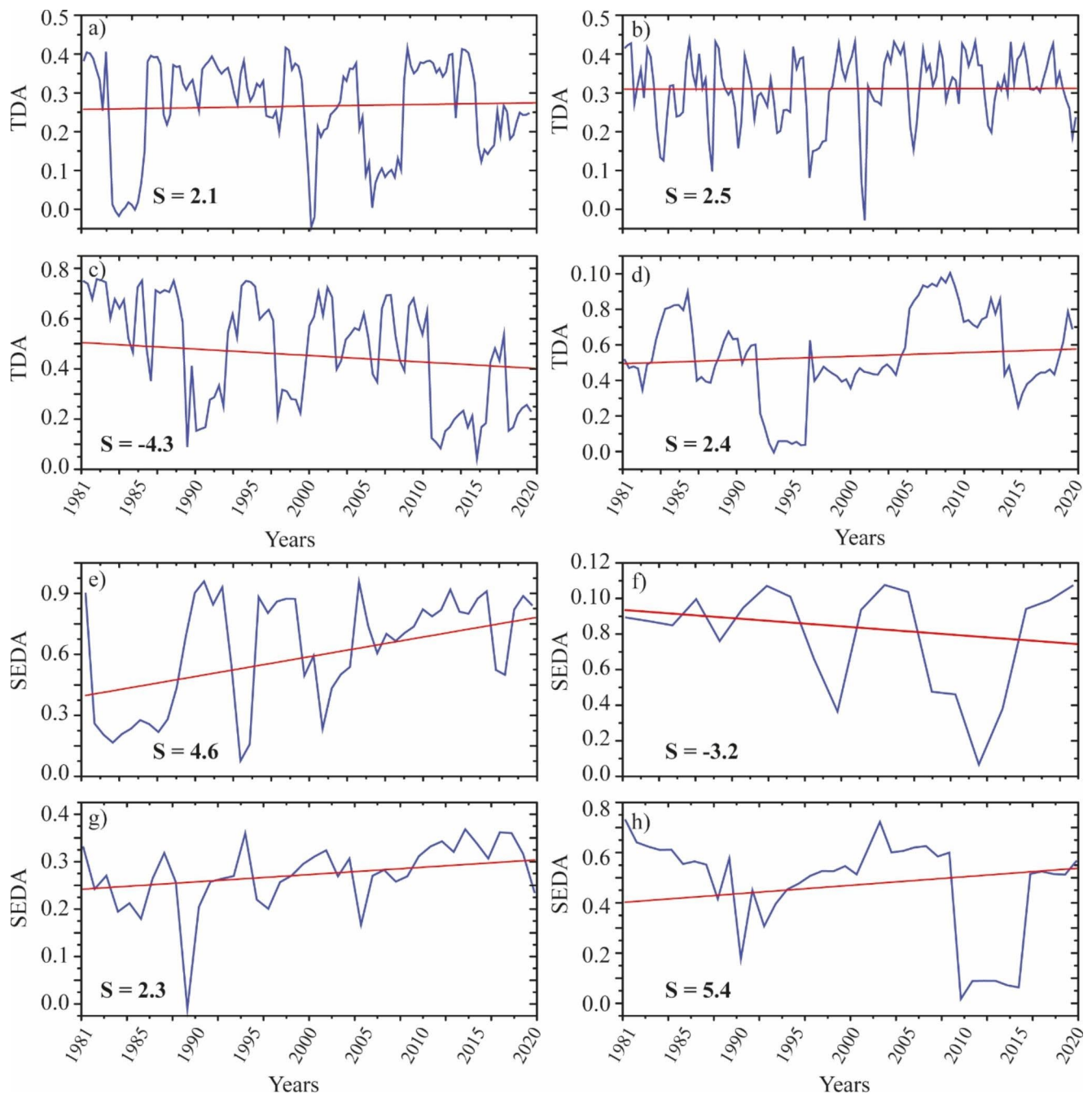


Fig. 7 Temporal distribution of annual total drought area (TDA) (a, b, c, d) and severe extreme drought area (SEDA) (e, f, g, h) for R1, R2, R3, and R4 of SA during 1981–2020, respectively. In temporal panels, the red line indicates a linear trend and S is the trend per decade using Sen's slope (S significant values are shown in each panel)

3.4 Composite analysis

Figure 8 illustrates the composite anomaly of air temperature, precipitation, PET, and their differences for two periods, 1981–2000 and 2001–2020, across SA. Figure 8a indicates that increased precipitation is obvious in the northern part of the SA, while the southeast part shows less precipitation. A robust increase is evident in precipitation over

the southwestern Himalayans during 1981–2000 (Fig. 8a), while a corresponding decrease is observed in the eastern Himalayans during 2001–2020 (Fig. 8b). For instance, east-western parts (Bhutan, Nepal, Bangladesh, and East India) showed substantial decreasing trends, also revealed by Almazroui et al. (2020). On the other hand, these regions exhibited increasing air temperature, particularly in the southern SA (Fig. 8c) (Aadhar and Mishra 2020). From the

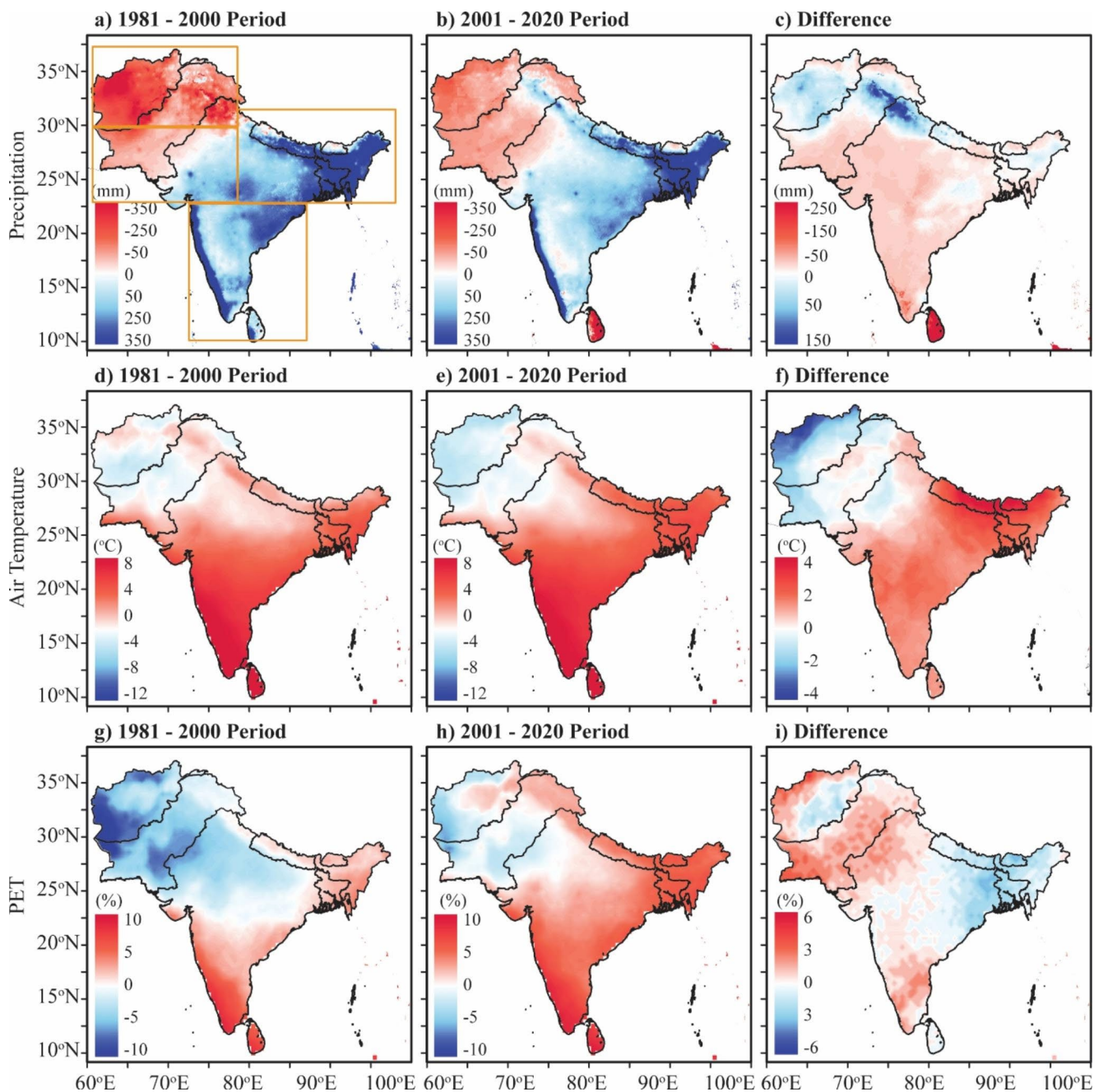


Fig. 8 Composite anomalies for precipitation (a, b), air temperature (d, e), potential evapotranspiration (PET: g, h), and their differences (c, f, i) during two target time periods such as 1981–2000 and 2000–2020, over SA, respectively. The light orange boxes in Fig. 8a represent the study subregions

results, it can be concluded that SA has gradually become wetter and warmer since the 1980s.

Based on the Clausius-Clapeyron relationship, the increase in air temperature over the study domain could increase the water holding capacity of the atmosphere, resulting in more extreme precipitation events for the region (Suman and Maity 2020). Using regional climate model over Pakistan, Rehman et al. (2018) projected a significant increase in mean temperature by around 6.5° under different

scenarios. It is noteworthy that the aforesaid studies have shown increased temperature and less precipitation over most parts of the SA, with higher intensity in the foothills of Himalayan, southern Pakistan, eastern Afghanistan, and western India. Furthermore, studies based on the down-scaling approach revealed a more warming climate over the high-altitude of SA and have correlated this warming trend with elevation-dependent warming (Preethi et al. 2019; Rana et al. 2020; Almazroui et al. 2020). It can be

remarked that the variations in air temperature suggested by these studies further clarify the credibility of our findings presented here.

During PET composite, Fig. 8 g–8 h revealed large variations over climate zones of SA during 1981–2000 and 2001–2020, respectively. For example, the period 1981–2000 is the lowest for hyper-arid and highest for the semi-arid regions compared to the 2001–2020 period. However, during semi-humid and arid regions, PET has increased while the other regions show a decline during the study period. The observed upsurge in PET in SA is significantly higher in the recent period than in the later period. The sensitivity of air temperature to PET is about 2 times higher than precipitation, and their differences for the majority of the climatic regions. The areal extent of severe droughts estimated using SPEI-PM compare well with the PET-based areal extent during the observed period. However, there are large differences in drought and PET estimates in extreme dry (hyperarid, arid) and wet (humid) regions (Fig. 8i).

Figure 8c and f, and 8i depict the differences in air temperature, precipitation, and PET for two periods between 1981 and 2000 and 2001–2020. The first time-period is subtracted from the final (time-period) to show the difference. Figure 8c show the precipitation variations between 1981 and 2000 and 2001–2020, which indicates the decreasing amounts of precipitation in the northern part of the region, while increased precipitation was found in the southern parts. Moreover, Fig. 8f indicates that the air temperature changes in the northwestern part of the SA are greater than that in the southeastern part of the region, which may affect the indicator of extreme regional temperature. The present study detected increasing trends of warm temperature events in the northern part of the regions, which agrees with the previous studies in the target regions (Niranjan et al. 2013; Ahmad et al. 2018). The increase of frequency and magnitude of daily extreme warm temperature and decrease of extreme cold temperature may occur in the global scope, resulting in an increase of length, frequency, and/or intensity of warm period or a heatwave in most land areas (Grimaldi et al. 2018). Compared with the driving factors of precipitation change at regional and global scales, the global average precipitation increases by ~2%/? of mean global warming in many parts of the world (Wang et al. 2014; Aadhar and Mishra 2020; Almazroui et al. 2020). Thus, the occurrences of severe and extreme droughts in four regions of SA have generally increased during 2001–2020, which could be due to the regional impact of global warming.

3.5 Multivariate drought return periods

To better understand the overall pattern of drought events and their association with meteorological drought, we used

bivariate quantiles (Isolines) (Hintze and Nelson 1998) to investigate the distribution of return periods based on drought duration and severity. The isolines represent the return period of drought with a different degree of severities over four subregions of SA from 1981 to 2020 (Fig. 9). In addition, the bivariate return period isolines are color-coded with joint density levels, where the blue color indicates lower densities and the red color represents higher densities ranging from 2-years to 100-years. The result showed that multivariate estimated values tend to increase under different return periods from R1 to R4 in terms of severity. For example, estimated R1 drought severity values fluctuate from 6 to 8-months with increased return periods from 5 to 20 years, while those of the R2, R3, and R4 vary from 5 to 7-months. The increasing ratio in computed values from 5 to 10-months is obvious, suggesting that the drought hazard is more severe in those target regions.

Furthermore, the interval of drought severity is wide, especially for high quantiles and/or large return periods. Consistent with estimated values, the median also increased significantly in all subregions, particularly in R1 and R3. Besides, the density increase is even more notable than that in the estimated values (at a rate of 6 to 10-months). For instance, the density of the drought severity range from 4 to 12-month for 50-, 70-, and 100-year return periods for the R1, whereas those of the R2, R3, and R4 drought severity range are between 2 to 8-months.

3.6 Large-scale climate drivers' relationships with meteorological drought events

The Pearson's correlation coefficients were estimated to check the preliminary outlook of the relationship between 12-month SPEI and seven selected large-scale climate indices across SA. Overall, DMI, IOD, and SST exhibited a strong positive correlation with 12-month SPEI, but PDO was negatively correlated with SPEI (Fig. 10). In the rest of the climate indices, the correlation coefficient varies with respect to lagged months. For instance, ENSO had negative correlations with 12-month SPEI in adjacent months (Aug. and Sept.), while a positive correlation can be seen for Niño3.4 in the same months. Similarly, Sunspots depict positive correlations in earlier months, whereas negative correlations can be seen in (Sept. and Oct.) months. It is noteworthy that previous years' climate indices could possibly have potential impacts on drought conditions (12-month SPEI) of the current year. On the other hand, the absolute r_p values are relatively small and around zero, suggesting that the relationship between large-scale climate drivers and 12-month SPEI was weak. Pearson's correlation coefficients only estimate the strength of the linear correlation between two time-series data. In subsequent analysis, we can use the

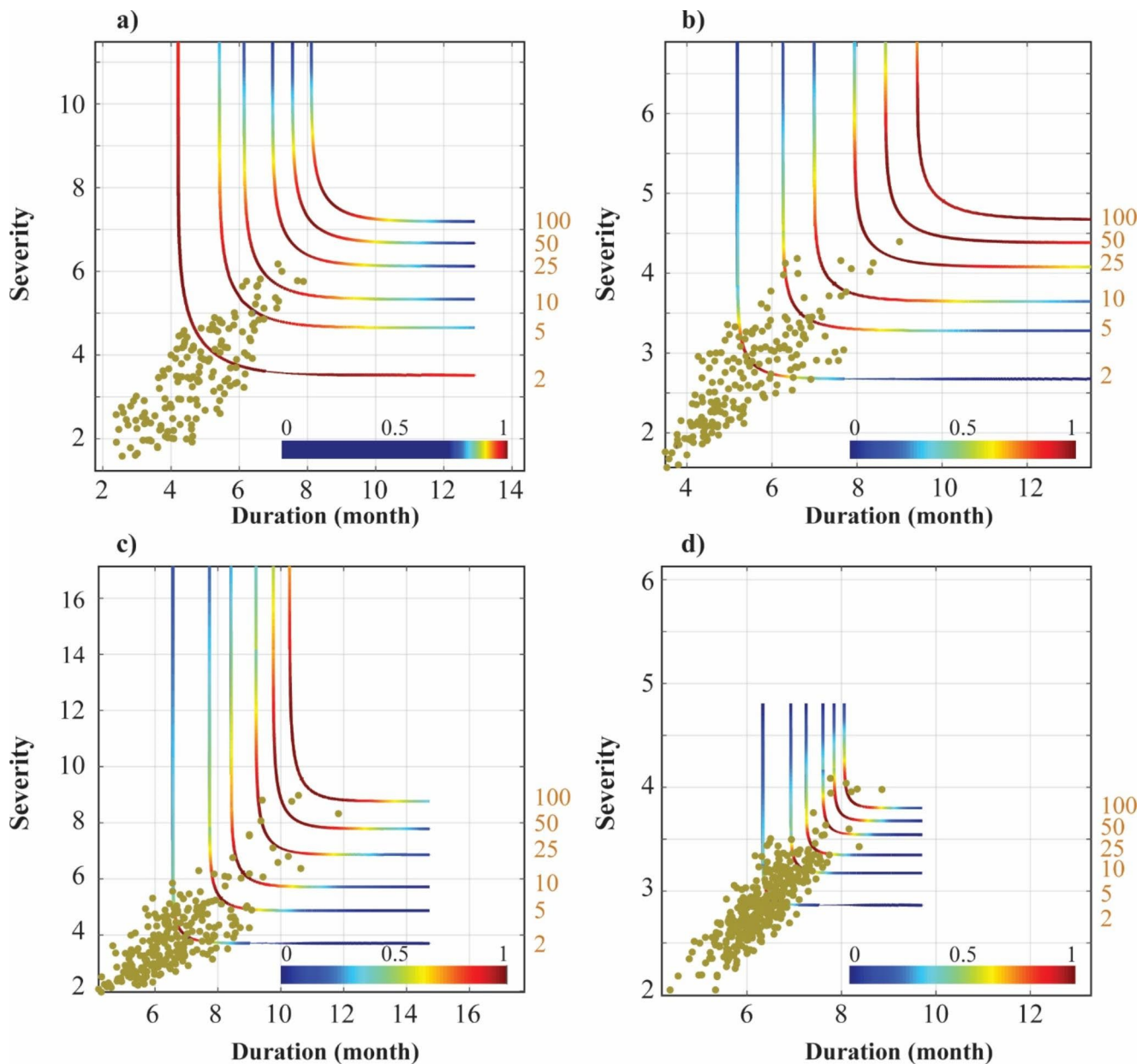


Fig. 9 The bivariate quantiles (Isolines) represent the return period of meteorological drought with a different degree of severities and duration ranging from 2-years to 100-years over the four distinct subregions of SA from 1981 to 2020 i.e., (a)-R1, (b)-R2, (c)-R3, and (d)-R4, respectively. In addition, the bivariate return period isolines are color-coded with joint density levels, where blue color indicates lower densities and the red color represents higher densities

BDL-model to explore other relationships, such as nonlinear correlations.

Figure 11 depicts the calculated dynamic regression slope coefficients of seven climate drivers on four distinct subregions of SA using the annual SPEI series. Figure 11a, h, and v shows that the correlations between DMI and SPEI at R1, R2, and R4 observed positive phase change after 1990 until 2020. For R3, the influence of the DMI has been relatively weak; however, a positive correlation is evident after a phase change circa 1995, while a negative correlation

can be seen after the 2000s (Fig. 11o), indicating a mitigated strength and possible phase change in near future. The positive phase of DMI and related geopotential height anomalies over SA provide an increase in the large-scale regional subsidence, causing dryer and warmer conditions (Shah and Mishra 2020a). Given predominant positive slope coefficients in R1, R2, and R4, where DMI exhibited positive phases since the 2000s, SPEI is expected to decline, resulting in a drier climate, particularly in southeastern SA. The findings concur with the previous work (Das et al. 2020),

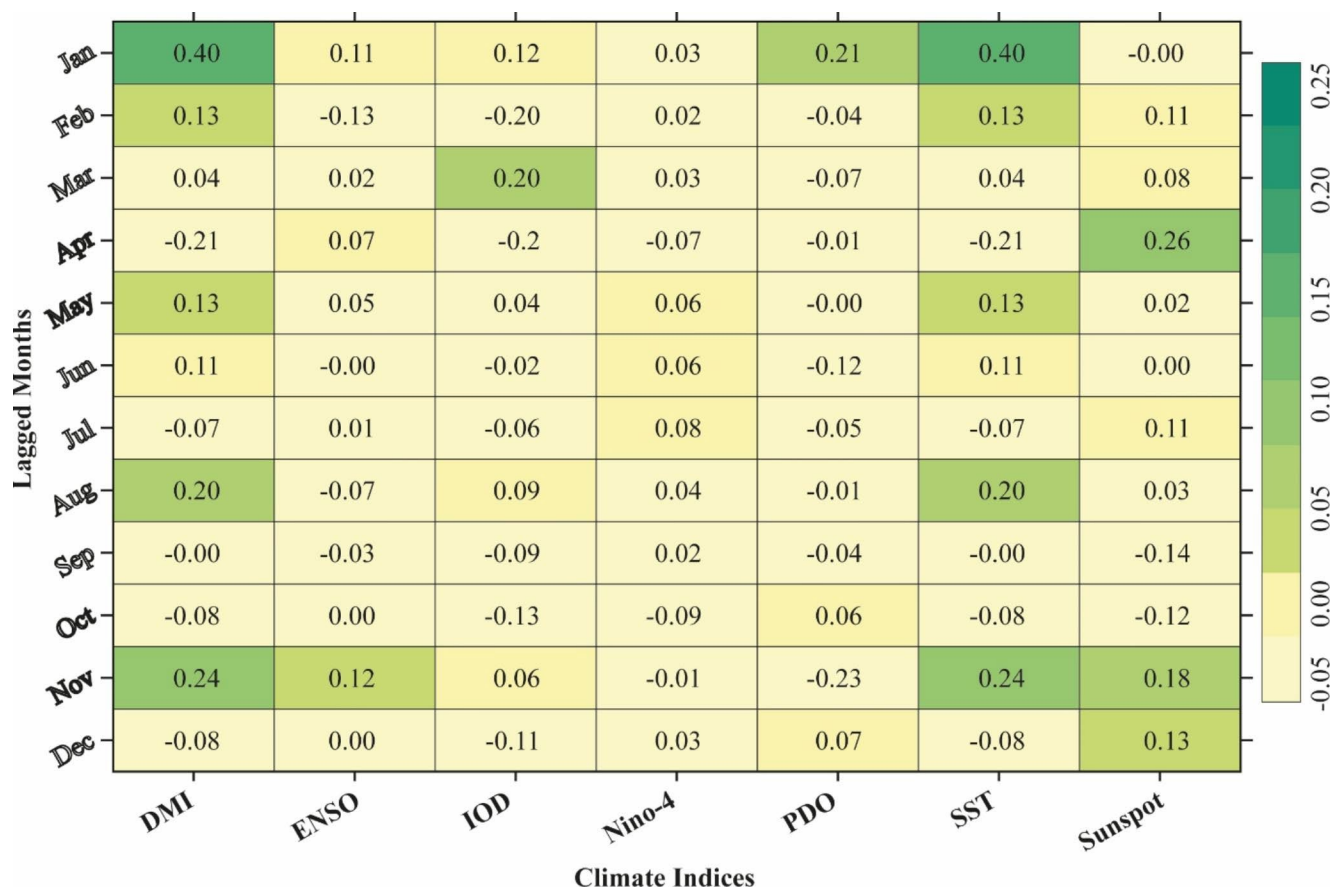


Fig. 10 Pearson's correlation coefficients matrix of the time series between monthly SPEI and lagged large-scale climate indices based on four distinct subregions across the SA sub-continent from 1981 to 2020. In 12-month SPEI (January to December) values of seven climate indices prior to the four target subregions were applied

which revealed that the strong positive (negative) phase of DMI could lead to the decrease (increase) in mean annual precipitation in southwestern SA.

ENSO is the most significant interannual climate pattern and plays an important role in global climate variability. In SA, El Niño is typically linked with drier winters, while La Niña has the vice-versa impacts. For instance, ENSO strongly impacts winter precipitation in southeast SA and El Niño may reduce the average winter precipitation by 12% (increase by 25%) (Almazroui et al. 2020). The cumulative role of the ENSO index, especially during monsoon season is perceived to affect the South Asian monsoon circulation pattern, thus resulting in dry/wet conditions during El Niño/La Niña years (Kang and Lee 2019). Our results further justify the time-varying impacts of ENSO on South Asian droughts (Fig. S4). A large negative slope coefficient could be seen for R1 and R2 during 2000–2010 (Fig. 11b and i). The robust impact of El Niño in those regions intend to a substantial decrease in SPEI values, which corresponds to the extreme severe droughts in SA countries during 2000–2005. The findings of (Joshi and Kar 2018) inferred similar

patterns during ENSO events, but they were rather limited to specific regions of SA (India).

For IOD, overall mixed behavior can be seen in all subregions; however, R1 and R2 depict increased slope coefficients from negative to positive circa between 1981 and 1990 (Fig. 11c and j), while an opposite association has occurred during 2010 for R3 and R4 (Fig. 11q and x). The impact of IOD in R1 stronger over the years, even though it remains negative. In addition, the slope coefficient for R2 changed circa 1990 from negative to positive (Fig. 11j). It can be seen from Fig. 11c that the warmer phase of IOD in the late 2000s attributed to a negative slope that leads to drier conditions in R1, while the cool phase between 2000 and 2010 showed a positive slope contributed to a wetter condition in R3, which is in agreement with previous research (Shah and Mishra 2020a). Moreover, IOD's warm period between 2010 and 2020 (the negative slope coefficient) may stimulate dryer conditions in R2, which may further exaggerate the extreme drought in southwestern SA from 2010 to 2020 (Fig. S4).

The correlation between Niño3.4 and SPEI at R1 evident a phase change from negative to positive (before 1981 to

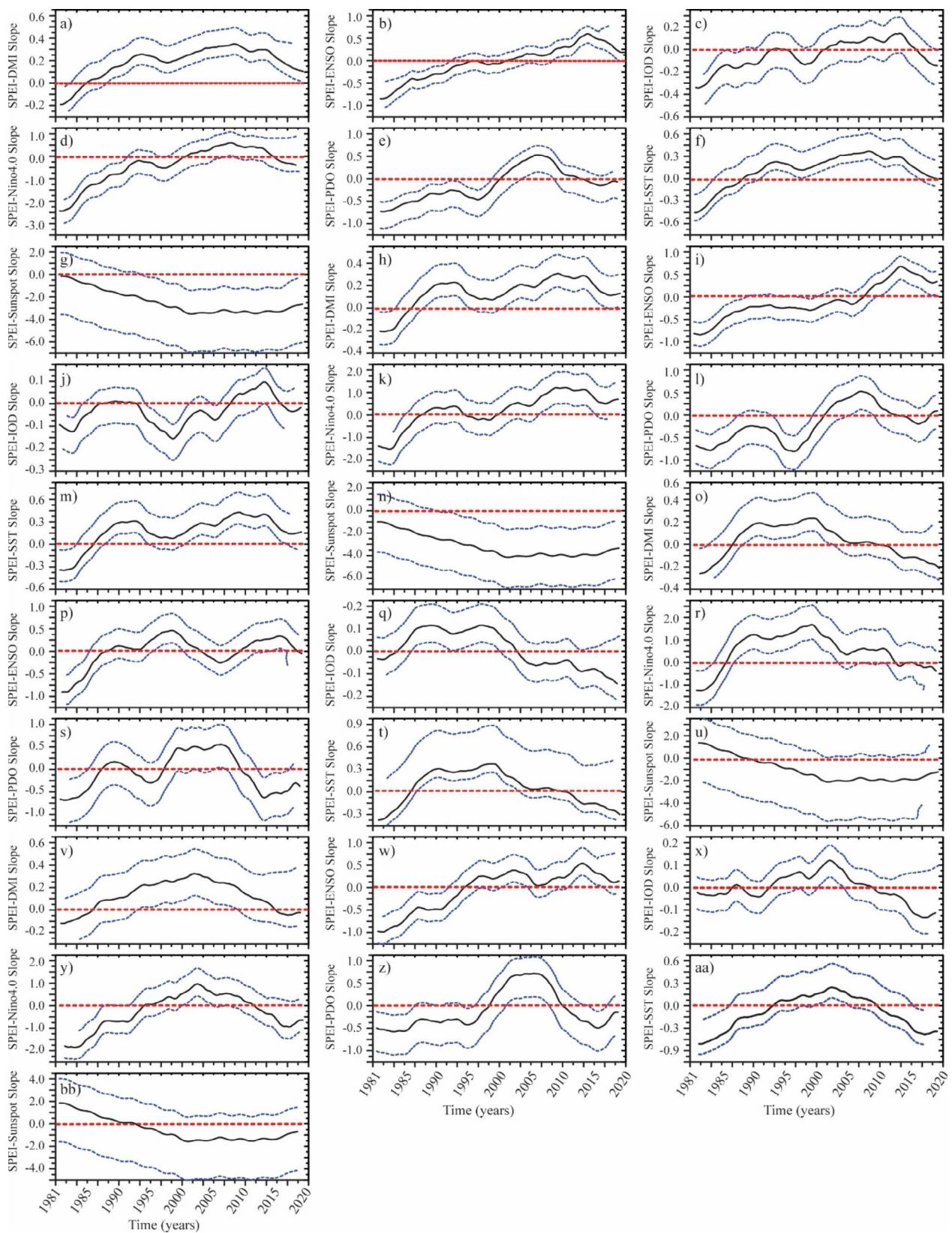


Fig. 11 Deviation in the relationship between regional SPEI (12-month) and seven large-scale climate indices fluctuations for R1 (a-g), R2 (h-n), R3 (o-u), and R4 (v-bb) across SA four subregions during 1981–2020, respectively. The solid black line in panels indicates the appraised time-varying slopes, along with the 25th and 75th percentile credible interval lines (red dashed lines) employing Bayesian Dynamic Linear (BDL) model

until the 1990s), while a negative change is observed after 1995 (Fig. 11d). Though complex behavior appeared in R2 where Niño3.4 was positively correlated with SPEI before the 1990s (Fig. 11k), there was a ridge circa 2000 and a trough during the 2010s. The slope coefficient detected a decadal variability in R3 from positive to negative, however, gradual change was observed after the 2000s (Fig. 11r). In addition, after the 2010s the slope coefficient of Niño3.4 tends to zero, suggesting that ENSO3.4's influence in all subregions of SA has been weakened in recent decades.

A phase change from negative to positive PDO was observed in R1 during 1990 and 2000 (Fig. 11e). Figure 11f revealed that PDO was negatively associated with 12-month SPEI; however, its effect declined from 1990 to 2020 in R2. A ridged circa was detected for both R3 and R4 during 2010 respectively, implying that PDO's impact was more severe (Fig. 11s). On the other hand, a relatively persistent negative phase change slope coefficient can be seen in R4 (Fig. 11z). Das et al. (2020) found that IOD's positive phase tends to be increased dry episodes during the growing season, particularly in southeastern SA. Another study by Mujumdar et al. (2020) reported that the northeast monsoon droughts are associated with a negative episode of IOD and ENSO (La Niña). Our results show that PDO is generally negatively correlated with SPEI (Fig. S4), which further justifies that a positive phase of PDO contributes to drying conditions in the target regions.

The distinct impacts of SST are obvious in R1, R3, and R4 from positive to negative during 2000 and 2010, respectively. In Fig. 11 m, a ridged slope change appeared in R2 from 2000 to 2020, whereas it seems that R2 experienced the stronger impact of SST at that time, while these effects decreased more after 2010 to a maximum until 2020. Besides, the slope coefficients after 2005 tend to reduce, indicating an impact of SST over R1, R3, and R4. Similarly, the correlation between SST and SPEI fluctuated in R4 during 2000–2020, which indicated a negative slope coefficient after the 2000s (Fig. 11aa). Our results further agree with the findings of Shah and Mishra (2020a). They reported that changes in drought variability in southeast SA are mainly associated with the SST anomalies in the Indian Ocean. These results affirm Kumar's (1999) findings, who stated that the interannual variation of Indian summer monsoon precipitation has strong relationship with the SST conditions over the Pacific and Indian Oceans.

The influence of Sunspots on annual SPEI seems to be generally stable and largely negative for most of the regions after the 2000s; however, the effect of Sunspots changed from positive to negative after the 2010s in R3 and R4, while greater negative slope coefficients can be seen after the 2000s for R2 (Fig. 11n). Interestingly, both R3 and R4 tend to increase slope coefficients after the 2010s, suggesting

Sunspots' reinforced effect in those regions in recent few decades. Our results confirm the findings of Zheng et al. (2017); they reported that the precipitation variability of high-altitude areas in northwest China is mostly affected by the Sunspots index to a large extent. The results further justify the findings of Fang et al. (2019), who described that the Sunspots index has an important role in strengthening China's dry conditions. It can be inferred from figure results that the predominantly negative correlation of Sunspots with SPEI over subregions of the SA indicated that the increase of Sunspots could lead to the decrease in SPEI, which further confirms that the dry events are most likely associated with the high intensity of Sunspots.

4 Discussions

Drought has a great influence on the regional hydro-meteorological cycle. The water source of rivers is more prone to drought events due to fewer human-induced activities (Guo et al. 2018; Omer et al. 2020). The higher temperature could change the snow/ice melting time during the drought period, while less/no change in precipitation over the mountainous region will reduce the snow cover in water-fed areas (Adnan et al. 2018; Huang et al. 2019; Liu et al. 2021). If the duration is long enough, insufficient precipitation and high temperature may enhance soil dryness, which ultimately negatively influences crop production and livestock health, increasing the demand for irrigation and aggravating the existing water crisis. On the other hand, river flow and lake storage decreased. In addition to river flow reduction, long-term drought events could be led to mitigating the groundwater level, with the most negative impacts on agriculture and fresh-water supply for domestic use (Guo et al. 2018; Das et al. 2020; Sein et al. 2022a). The rise in the Arabian Sea's dryness is mainly caused by incursion deviation for irrigation and decreased precipitation (Hina et al. 2021; Sein et al. 2022b). They also found that dryness significantly increased over the Gangetic Plain and southern Pakistan from 1950 to 2016. Our study further confirms the previous work. It is observed that the southwest and northeast SA subregions suffered from prolonged drying trends and detected more drought events with long-lasting duration and higher severity. It is noteworthy that an obvious TDF and SEDS (Fig. 4), as well as the prolonged drying trend with intensified magnitude (Figs. 6 and 7), appeared in the last 15 years (2000–2015). Therefore, policymakers and disaster risk managers must take serious measures to avoid more negative impacts.

Climate change and human-induced influences could cause non-stationarities in hydro-meteorological extremes (Miyan 2015; Shahzaman et al. 2021a; Iyakaremye et al.

2021). Global atmospheric circulation and abrupt climate variability have been detected (Gu et al. 2020b); e.g., the pattern of the summer monsoon rainfall over SA showed a declining trend from 2001 to 2020, but then increased sharply (Latif et al. 2017; Mie Sein et al. 2021b; Ullah et al. 2021). During the 2000s, various phase changes appeared for the dynamic regression slope coefficients, which might be attributed to the unusual climatic pattern during the 2010s considering the substantial shift from wetter (cooler) to drier (warmer) subtropical Pacific SSTs. Using principal component (PC), Shah and Mishra, (2020a) found a strong correlation of SST with the first PC over the tropical southern Atlantic Ocean; however, they also noticed that warming in the Indian Ocean has resulted in droughts over Gangetic Plain while the western parts of SA experienced a wetter trend. Our results further support the findings of Latif et al. (2017). They reported that the subtropical phenomena might affect the average monsoon precipitation trend over southwestern SA by enhanced cross-equatorial moisture transport into the Arabian Sea.

The study further explored the role of large-scale oceanic and atmospheric circulation patterns as a potential driver of such trends. The robust BDL-model was used to investigate the possible association of large-scale climate drivers with 12-month SPEI. Results revealed that an obvious relationship of ENSO events was observed with SPEI, as well as IOD and La-Niña onset timing as explored for some areas of SA, especially eastern India and Bangladesh (Adnan et al. 2016; Sun and Liu 2019; Mie Sein et al. 2021a). Moreover, a consistently weaker phase of positive IOD and PDO patterns during the recent severe drought in 2000–2005 deviates from the previous drought (Fig. S4), which tends to be linked with large-scale connections (Xiao et al. 2019; Ain et al. 2020; Liu et al. 2020). Rajagopalan et al. (2000) explored the association of droughts with ENSO over the past summer U.S. They suggested applying the BDL model to understand better the non-stationary relationship between droughts and ENSO during the 20th century. Meanwhile, Yang et al. (2020) studied the influence of climate drivers on regional drought variability using the BDL model. They described that droughts are generally more negatively correlated with PDO and ENSO and more positively correlated with SST and DMI after the 1990s. The findings infer the possibility that the precipitation variability over SA has less/not-significant association with ENSO, IOD, and monsoon onset timing. The trend in precipitation could be due to extreme events, their respective intensity and frequency during each month, which could perhaps have had, is the driver. Even though the large-scale indices may have little impact, the influence of Tibetan Plateau thermal controls and Himalayan forcing may need to be thoroughly investigated.

It can be inferred that the dynamic influences of large-scale climate circulations on meteorological droughts in SA evident significant changes in the relationships. Even though substantially decreased exposure to large-scale climate drivers' the most severe influences appeared on droughts events such as duration, area, intensity, frequency, and severity. The study results, i.e., the spatial and temporal drought features, trend, return periods, periodicity of drought, and its relationship with large-scale climate indices, will provide useful information for disaster risk managers and policymakers.

5 Conclusion

To better understand the importance of the spatiotemporal variability of drought characteristics to mitigate drought risk, this study intends to comprehensively assess SA's drought conditions. The gauge-based gridded CRU TS4.05 and CHIRPS datasets were used to compute secular SPEI index (3-month and 12-month) for seasonal and annual timescale over four homogenous subregions of SA during 1981–2020. A series of drought events, including drought area, duration, intensity, frequency, and severity, are thoroughly investigated using Run theory, while k-means clustering was adopted for regionalization. Moreover, the trend magnitude was detected using the nonparametric Sen's Slope estimator and the modified-MK approach. Finally, the possible links between drought variability and large-scale climate drivers are assessed based on Pearson's correlation coefficient and BDL-model. A summary of the findings is as follows:

- 1) In terms of seasonal variability, the impacts of severe and long-lasting droughts events appeared from 2000 to 2010. A predominant wetting trend was exhibited during the spring and autumn seasons over most regions of SA, but a widespread drying trend can be seen in the summer season while the drought risk in the winter season has worsened.
- 2) During TDF and SEDF, the south and northern SA appeared with more severe drought events covering R1 and R2. However, a slight increase can be seen in R3 than R4.
- 3) A complex behavior was revealed during TDD and LDD; however, the western parts of SA exhibit longer drought duration while shorter duration could be seen in southern parts. Spatially, a significant declining trend was observed in R3 and R4 for TDD. In terms of the temporal trend, a drought occurred largely from 1990 to 2010 across SA, while R1 detected an increasing trend during the 2000s. Overall, SEDD observed a significantly decreasing trend in most subregions, which could

be attributed to TDD's significant general decrease over east and northern SA.

- 4) TDS observed prevalent positive trends, particularly in R1 and R2 than R3 and R4, suggesting that droughts relatively increased from 1990 to 2020. A similar pattern can also be seen for SEDS in those regions, whereas most subregions suffered from extremely severe droughts after the 2000s. It can be concluded that the overall increase in SEDS could result in a general rise in annual TDS across SA.
- 5) This study further explored the dynamic impact of large-scale climate drivers on meteorological droughts over four subregions of SA. Generally, DMI and ENSO's influence was relatively stronger after the 2000s over most subregions of SA in recent decades, while phase change was detected for Niño, PDO, and SST during the 2000s, and 2010s, respectively. ENSO, SST, IOD, and DMI cycles have a prominent effect on drought variability based on SPEI in all subregions of the SA. Additionally, SST anomalies in the Indian and the Pacific oceans affect the regional scale droughts in SA (i.e., Pakistan, Afghanistan, Bangladesh, and India).

Acknowledgements The authors greatly acknowledge the financial support of the National Natural Science Foundation of China (41877158). We are thankful to all datasets centers for availing data to use in drought monitoring and their potential climate driver's studies over South Asia. We would like to thank anonymous reviewers for their valuable time and courtesy.

References

- Aadhar S, Mishra V (2020) Increased drought risk in South Asia under warming climate: Implications of uncertainty in potential evapotranspiration estimates. *J Hydrometeorol*. <https://doi.org/10.1175/jhm-d-19-0224.1>
- Aadhar S, Mishra V (2019) A substantial rise in the area and population affected by dryness in South Asia under 1.5°C, 2.0°C and 2.5°C warmer worlds. *Environ Res Lett* 14:114021. <https://doi.org/10.1088/1748-9326/ab4862>
- Adnan S, Ullah K, Shouting G (2016) Investigations into precipitation and drought climatologies in south central Asia with special focus on Pakistan over the period 1951–2010. *J Clim* 29:6019–6035. <https://doi.org/10.1175/JCLI-D-15-0735.1>
- Adnan S, Ullah K, Shuanglin L et al (2018) Comparison of various drought indices to monitor drought status in Pakistan. *Clim Dyn* 51:1885–1899. <https://doi.org/10.1007/s00382-017-3987-0>
- Ahmad I, Zhang F, Tayyab M et al (2018) Spatiotemporal analysis of precipitation variability in annual, seasonal and extreme values over upper Indus River basin. *Atmos Res* 213:346–360. <https://doi.org/10.1016/j.atmosres.2018.06.019>
- Ahmed K, Shahid S, Chung E et al (2019a) Climate change uncertainties in seasonal drought severity-area-frequency curves: Case of arid region of Pakistan. *J Hydrol* 570:473–485. <https://doi.org/10.1016/j.jhydrol.2019.01.019>
- Ahmed K, Shahid S, Nawaz N (2018) Impacts of climate variability and change on seasonal drought characteristics of Pakistan. *Atmos Res* 214:364–374. <https://doi.org/10.1016/j.atmosres.2018.08.020>
- Ahmed K, Shahid S, Wang X et al (2019b) Spatiotemporal changes in aridity of Pakistan during 1901–2016. *Hydrol Earth Syst Sci* 23:3081–3096. <https://doi.org/10.5194/hess-23-3081-2019>
- Ain N, Latif M, Ullah K et al (2020) Investigation of seasonal droughts and related large-scale atmospheric dynamics over the Potwar Plateau of Pakistan. *Theor Appl Climatol* 140:69–89. <https://doi.org/10.1007/s00704-019-03064-8>
- Ali S, Henchiri M, Yao F, Zhang J (2019) Analysis of vegetation dynamics, drought in relation with climate over South Asia from 1990 to 2011. *Environ Sci Pollut Res* 26:11470–11481. <https://doi.org/10.1007/s11356-019-04512-8>
- Allen R, Smith M, Pereira L, Perrier A (1994) An Update for the Calculation of Reference Evapotranspiration. *ICID Bull*
- Almazroui M, Saeed S, Saeed F et al (2020) Projections of Precipitation and Temperature over the South Asian Countries in CMIP6. *Earth Syst Environ* 4:297–320. <https://doi.org/10.1007/s41748-020-00157-7>
- Arshad M, Ma X, Yin J et al (2021a) Performance evaluation of ERA-5, JRA-55, MERRA-2, and CFS-2 reanalysis datasets, over diverse climate regions of Pakistan. *Weather Clim Extrem* 33:100373. <https://doi.org/10.1016/j.wace.2021.100373>
- Arshad M, Ma X, Yin J et al (2021b) Evaluation of GPM-IMERG and TRMM-3B42 precipitation products over Pakistan. *Atmos Res* 249:105341. <https://doi.org/10.1016/j.atmosres.2020.105341>
- Bevan J, Kendall M (1971) Rank Correlation Methods. *Stat* 20:74. <https://doi.org/10.2307/2986801>
- Dai A (2011) Characteristics and trends in various forms of the Palmer Drought Severity Index during 1900–2008. *J Geophys Res Atmos* 116. <https://doi.org/10.1029/2010JD015541>
- Das J, Jha S, Goyal M (2020) Non-stationary and copula-based approach to assess the drought characteristics encompassing climate indices over the Himalayan states in India. *J Hydrol* 580:124356. <https://doi.org/10.1016/j.jhydrol.2019.124356>
- Diaz V, Corzo G, Van Lanen H et al (2020) An approach to characterise spatio-temporal drought dynamics. *Adv Water Resour* 137:103512. <https://doi.org/10.1016/j.advwatres.2020.103512>
- Fang W, Huang S, Huang G et al (2019) Copulas-based risk analysis for inter-seasonal combinations of wet and dry conditions under a changing climate. *Int J Climatol*. <https://doi.org/10.1002/joc.5929>
- Frank A, Armenski T, Gocic M et al (2017) Influence of mathematical and physical background of drought indices on their complementarity and drought recognition ability. *Atmos Res*. <https://doi.org/10.1016/j.atmosres.2017.05.006>
- Gaire N, Dhakal Y, Shah S et al (2019) Drought (scPDSI) reconstruction of trans-Himalayan region of central Himalaya using *Pinus wallichiana* tree-rings. *Palaeogeogr Palaeoclimatol Palaeoecol* 514:251–264. <https://doi.org/10.1016/j.palaeo.2018.10.026>
- Gao T, Wang H, Zhou T (2017) Changes of extreme precipitation and nonlinear influence of climate variables over monsoon region in China. *Atmos Res* 197:379–389. <https://doi.org/10.1016/j.atmosres.2017.07.017>
- Gebremeskel Haile G, Tang Q, Leng G et al (2020) Long-term spatio-temporal variation of drought patterns over the Greater Horn of Africa. *Sci Total Environ* 704:135299. <https://doi.org/10.1016/j.scitotenv.2019.135299>
- Grimaldi S, Petroselli A, Baldini L, Gorgucci E (2018) Description and preliminary results of a 100 square meter rain gauge. *J Hydrol* 556:827–834. <https://doi.org/10.1016/j.jhydrol.2015.09.076>
- Gu L, Chen J, Xu C et al (2019) The contribution of internal climate variability to climate change impacts on droughts. *Sci Total Environ* 684:229–246. <https://doi.org/10.1016/j.scitotenv.2019.05.345>
- Gu L, Chen J, Yin J et al (2020a) Drought hazard transferability from meteorological to hydrological propagation. *J Hydrol* 585:124761. <https://doi.org/10.1016/j.jhydrol.2020.124761>
- Gu L, Chen J, Yin J et al (2020b) Projected increases in magnitude and socioeconomic exposure of global droughts in 1.5 and 2°C

- warmer climates. *Hydrol Earth Syst Sci* 24:451–472. <https://doi.org/10.5194/hess-24-451-2020>
- Guo H, Bao A, Liu T et al (2018) Spatial and temporal characteristics of droughts in Central Asia during 1966–2015. *Sci Total Environ* 624:1523–1538. <https://doi.org/10.1016/j.scitotenv.2017.12.120>
- Guo H, Bao A, Liu T et al (2019) Determining variable weights for an Optimal Scaled Drought Condition Index (OSDCI): Evaluation in Central Asia. *Remote Sens Environ* 231:111220. <https://doi.org/10.1016/j.rse.2019.111220>
- Gupta V, Jain M (2018) Investigation of multi-model spatiotemporal mesoscale drought projections over India under climate change scenario. *J Hydrol* 567:489–509. <https://doi.org/10.1016/j.jhydrol.2018.10.012>
- Hamed K, Rao A (1998) A modified Mann-Kendall trend test for auto-correlated data. *J Hydrol* 204:182–196. [https://doi.org/10.1016/S0022-1694\(97\)00125-X](https://doi.org/10.1016/S0022-1694(97)00125-X)
- Hao Z, AghaKouchak A (2013) Multivariate Standardized Drought Index: A parametric multi-index model. *Adv Water Resour* 57:12–18. <https://doi.org/10.1016/j.advwatres.2013.03.009>
- Hina S, Saleem F, Arshad A et al (2021) Droughts over Pakistan: possible cycles, precursors and associated mechanisms. *Geomat. Nat Hazards Risk* 12:1638–1668. <https://doi.org/10.1080/19475705.2021.1938703>
- Hintze J, Nelson R (1998) Violin Plots: A Box Plot-Density Trace Synergism. *Am Stat* 52:181–184. <https://doi.org/10.1080/00031305.1998.10480559>
- Hoerling M, Eischeid J, Kumar A et al (2014) Causes and predictability of the 2012 great plains drought. *Bull Am Meteorol Soc.* <https://doi.org/10.1175/BAMS-D-13-00055.1>
- Huang S, Wang L, Wang H et al (2019) Spatio-temporal characteristics of drought structure across China using an integrated drought index. *Agric Water Manag* 218:182–192. <https://doi.org/10.1016/j.agwat.2019.03.053>
- Iyakaremye V, Zeng G, Ullah I et al (2022) Recent Observed Changes in Extreme High-Temperature Events and Associated Meteorological Conditions over Africa. *Int J Climatol* 1–16. <https://doi.org/10.1002/joc.7485>
- Iyakaremye V, Zeng G, Yang X et al (2021) Increased high-temperature extremes and associated population exposure in Africa by the mid-21st century. *Sci Total Environ* 790:148162. <https://doi.org/10.1016/j.scitotenv.2021.148162>
- Jiang J, Zhou T, Chen X, Zhang L (2020) Future changes in precipitation over Central Asia based on CMIP6 projections. *Environ Res Lett* 15:054009. <https://doi.org/10.1088/1748-9326/ab7d03>
- Jiang S, Wei L, Ren L et al (2021) Utility of integrated IMERG precipitation and GLEAM potential evapotranspiration products for drought monitoring over mainland China. *Atmos Res* 247:105141. <https://doi.org/10.1016/j.atmosres.2020.105141>
- Joshi S, Kar S (2018) Mechanism of ENSO influence on the South Asian monsoon rainfall in global model simulations. *Theor Appl Climatol* 131:1449–1464. <https://doi.org/10.1007/s00704-017-2045-5>
- Kang D, Lee M (2019) ENSO influence on the dynamical seasonal prediction of the East Asian Winter Monsoon. *Clim Dyn* 53:7479–7495. <https://doi.org/10.1007/s00382-017-3574-4>
- Khan N, Sachindra D, Shahid S et al (2020) Prediction of droughts over Pakistan using machine learning algorithms. *Adv Water Resour* 139. <https://doi.org/10.1016/j.advwatres.2020.103562>
- Khatiwada K, Pandey V (2019) Characterization of hydro-meteorological drought in Nepal Himalaya: A case of Karnali River Basin. *Weather Clim Extrem* 26:100239. <https://doi.org/10.1016/j.wace.2019.100239>
- Kishore P, Jyothi S, Basha G et al (2016) Precipitation climatology over India: validation with observations and reanalysis datasets and spatial trends. *Clim Dyn* 46:541–556. <https://doi.org/10.1007/s00382-015-2597-y>
- Latif M, Hannachi A, Syed F (2018) Analysis of rainfall trends over Indo-Pakistan summer monsoon and related dynamics based on CMIP5 climate model simulations. *Int J Climatol* 38:e577–e595. <https://doi.org/10.1002/joc.5391>
- Latif M, Syed F, Hannachi A (2017) Rainfall trends in the South Asian summer monsoon and its related large-scale dynamics with focus over Pakistan. *Clim Dyn* 48:3565–3581. <https://doi.org/10.1007/s00382-016-3284-3>
- Liu B, Chen X, Li Y, Chen X (2018) Long-term change of potential evapotranspiration over southwest China and teleconnections with large-scale climate anomalies. *Int J Climatol* 38:1964–1975. <https://doi.org/10.1002/joc.5309>
- Liu B, Wu G, Ren R (2015) Influences of ENSO on the vertical coupling of atmospheric circulation during the onset of South Asian summer monsoon. *Clim Dyn* 45:1859–1875. <https://doi.org/10.1007/s00382-014-2439-3>
- Liu M, Ma X, Yin Y et al (2021) Non-stationary frequency analysis of extreme streamflow disturbance in a typical ecological function reserve of China under a changing climate. *Ecohydrology* 23:1–20. <https://doi.org/10.1002/eco.2323>
- Liu W, Zhu S, Huang Y et al (2020) Spatiotemporal Variations of Drought and Their Teleconnections with Large-Scale Climate Indices over the Poyang Lake Basin, China. *Sustainability* 12:3526. <https://doi.org/10.3390/su12093526>
- Lu B, Ren H-L, Eade R, Andrews M (2018) Indian Ocean SST modes and Their Impacts as Simulated in BCC_CSM1.1(m) and Had-GEM3. *Adv Atmos Sci* 35:1035–1048. <https://doi.org/10.1007/s00376-018-7279-3>
- Mann HB (1945) Nonparametric Tests Against Trend. *Econometrica* 13:245–259. <https://doi.org/10.2307/1907187>
- McKee TB, Nolan J, Kleist J (1993) The relationship of drought frequency and duration to time scales. *Prepr Eighth Conf Appl Climatol Amer Meteor, Soc*
- Mie Sein Z, Ullah I, Syed S et al (2021a) Interannual Variability of Air Temperature over Myanmar: The Influence of ENSO and IOD. *Climate* 9:35. <https://doi.org/10.3390/cli9020035>
- Mie Sein ZM, Ullah I, Saleem F et al (2021b) Interdecadal Variability in Myanmar Rainfall in the Monsoon Season (May–October) Using Eigen Methods. *Water* 13:729. <https://doi.org/10.3390/w13050729>
- Mishra A, Singh V (2010) A review of drought concepts. *J Hydrol* 391:202–216. <https://doi.org/10.1016/j.jhydrol.2010.07.012>
- Mishra V, Bhatia U, Tiwari A (2020) Bias-corrected climate projections from Coupled Model Intercomparison Project-6 (CMIP6) for South Asia. 6
- Mishra V, Shah R, Azhar S, et al (2017) Reconstruction of droughts in India using multiple land surface models (1951–2015). *Hydrol Earth Syst Sci Discuss* 1–22. <https://doi.org/10.5194/hess-2017-302>
- Miyam M (2015) Droughts in Asian Least Developed Countries: Vulnerability and sustainability. *Weather Clim Extrem* 7:8–23. <https://doi.org/10.1016/j.wace.2014.06.003>
- Mohsenipour M, Shahid S, Chung E, Wang X (2018) Changing Pattern of Droughts during Cropping Seasons of Bangladesh. *Water Resour Manag* 32:1555–1568. <https://doi.org/10.1007/s11269-017-1890-4>
- Mujumdar M, Bhaskar P, Ramarao M et al (2020) Assessment of Climate Change over the Indian Region. Springer Singapore, Singapore
- Niranjan K, Rajeevan M, Pai D et al (2013) On the observed variability of monsoon droughts over India. *Weather Clim Extrem* 1:42–50. <https://doi.org/10.1016/j.wace.2013.07.006>
- Omer A, Elagib N, Zhuguo M et al (2020) Water scarcity in the Yellow River Basin under future climate change and human activities. *Sci Total Environ* 749:141446. <https://doi.org/10.1016/j.scitotenv.2020.141446>

- Palmer WC (1965) Meteorological Drought. U.S. Weather Bur. Res Pap No 45:58
- Pathak A, Ghosh S, Martinez J et al (2017) Role of Oceanic and Land Moisture Sources and Transport in the Seasonal and Interannual Variability of Summer Monsoon in India. *J Clim* 30:1839–1859. <https://doi.org/10.1175/JCLI-D-16-0156.1>
- Pettitt AN (1979) A Non-Parametric Approach to the Change-Point Problem. *Appl Stat*. <https://doi.org/10.2307/2346729>
- Preethi B, Ramya R, Patwardhan S et al (2019) Variability of Indian summer monsoon droughts in CMIP5 climate models. *Clim Dyn* 53:1937–1962. <https://doi.org/10.1007/s00382-019-04752-x>
- Qutbudin I, Shiru M, Sharafati A et al (2019) Seasonal Drought Pattern Changes Due to Climate Variability: Case Study in Afghanistan. *Water* 11:1096. <https://doi.org/10.3390/w11051096>
- Rana A, Nikulin G, Kjellström E et al (2020) Contrasting regional and global climate simulations over South Asia. *Clim Dyn* 54:2883–2901. <https://doi.org/10.1007/s00382-020-05146-0>
- Rehman N, Adnan M, Ali S (2018) Assessment of CMIP5 climate models over South Asia and climate change projections over Pakistan under representative concentration pathways. *Int J Glob Warm* 16:381. <https://doi.org/10.1504/IJGW.2018.095994>
- Sajjad MM, Wang J, Abbas H et al (2022) Impact of Climate and Land-Use Change on Groundwater Resources, Study of Faisalabad District, Pakistan. *Atmos (Basel)* 13:1097. <https://doi.org/10.3390/atmos13071097>
- Seager R, Hoerling M, Schubert S et al (2015) Causes of the 2011–14 California drought. *J Clim*. <https://doi.org/10.1175/JCLI-D-14-00860.1>
- Sein ZMM, Ullah I, Iyakaremye V et al (2022a) Observed spatiotemporal changes in air temperature, dew point temperature and relative humidity over Myanmar during 2001–2019. *Meteorol Atmos Phys* 134:7. <https://doi.org/10.1007/s00703-021-00837-7>
- Sein ZMM, Zhi X, Ullah I et al (2022b) Recent variability of sub-seasonal monsoon precipitation and its potential drivers in Myanmar using in-situ observation during 1981–2020. *Int J Climatol* 42:3341–3359. <https://doi.org/10.1002/joc.7419>
- Sen P (1968) Estimates of the Regression Coefficient Based on Kendall's Tau. *J Am Stat Assoc* 63:1379–1389. <https://doi.org/10.1080/01621459.1968.10480934>
- Shah D, Mishra V (2020a) Drought Onset and Termination in India. *J Geophys Res Atmos* 125:1–21. <https://doi.org/10.1029/2020JD032871>
- Shah D, Mishra V (2020b) Integrated Drought Index (IDI) for Drought Monitoring and Assessment in India. *Water Resour Res* 56:1–22. <https://doi.org/10.1029/2019WR026284>
- Shahzaman M, Zhu W, Bilal M et al (2021a) Remote Sensing Indices for Spatial Monitoring of Agricultural Drought in South Asian Countries. *Remote Sens* 13:2059. <https://doi.org/10.3390/rs13112059>
- Shahzaman M, Zhu W, Ullah I et al (2021b) Comparison of Multi-Year Reanalysis, Models, and Satellite Remote Sensing Products for Agricultural Drought Monitoring over South Asian Countries. *Remote Sens* 13:3294. <https://doi.org/10.3390/rs13163294>
- Sheffield J, Wood EF, Roderick ML (2012) Little change in global drought over the past 60 years. *Nature* 491:435–438. <https://doi.org/10.1038/nature11575>
- Sheikh M, Manzoor N, Ashraf J et al (2015) Trends in extreme daily rainfall and temperature indices over South Asia. *Int J Climatol* 35:1625–1637. <https://doi.org/10.1002/joc.4081>
- Shukla S, Wood AW (2008) Use of a standardized runoff index for characterizing hydrologic drought. *Geophys Res Lett* 35:L02405. <https://doi.org/10.1029/2007GL032487>
- Suman M, Maity R (2020) Southward shift of precipitation extremes over south Asia: Evidences from CORDEX data. *Sci Rep* 10:6452. <https://doi.org/10.1038/s41598-020-63571-x>
- Sun C, Liu Y (2019) Tree-ring-based drought variability in the eastern region of the Silk Road and its linkages to the Pacific Ocean. *Ecol Indic* 96:421–429. <https://doi.org/10.1016/j.ecolind.2018.09.032>
- Thornthwaite C (1948) An Approach toward a Rational Classification of Climate. *Geogr Rev* 38:55. <https://doi.org/10.2307/210739>
- Ullah I, Ma X, Ren G et al (2022a) Recent Changes in Drought Events over South Asia and Their Possible Linkages with Climatic and Dynamic Factors. *Remote Sens* 14:3219. <https://doi.org/10.3390/rs14133219>
- Ullah I, Ma X, Yin J et al (2022b) Observed changes in seasonal drought characteristics and their possible potential drivers over Pakistan. *Int J Climatol* 42:1576–1596. <https://doi.org/10.1002/joc.7321>
- Ullah I, Ma X, Yin J et al (2021) Evaluating the meteorological drought characteristics over Pakistan using in situ observations and reanalysis products. *Int J Climatol* 41:4437–4459. <https://doi.org/10.1002/joc.7063>
- Ullah I, Saleem F, Iyakaremye V et al (2022c) Projected Changes in Socioeconomic Exposure to Heatwaves in South Asia Under Changing Climate. *Earth's Futur* 10:1–19. <https://doi.org/10.1029/2021EF002240>
- Ummerhofer C, D'Arrigo R, Anchukaitis K et al (2013) Links between Indo-Pacific climate variability and drought in the Monsoon Asia Drought Atlas. *Clim Dyn* 40:1319–1334. <https://doi.org/10.1007/s00382-012-1458-1>
- Uwimbabazi J, Jing Y, Iyakaremye V et al (2022) Observed Changes in Meteorological Drought Events during 1981–2020 over Rwanda, East Africa. *Sustainability* 14:1519. <https://doi.org/10.3390/su14031519>
- Vangelis H, Tigkas D, Tsakiris G (2013) The effect of PET method on Reconnaissance Drought Index (RDI) calculation. *J Arid Environ* 88:130–140. <https://doi.org/10.1016/j.jaridenv.2012.07.020>
- Vicente-Serrano S, Beguería S, López-Moreno J (2010) A Multiscalar Drought Index Sensitive to Global Warming: The Standardized Precipitation Evapotranspiration Index. *J Clim* 23:1696–1718. <https://doi.org/10.1175/2009JCLI2909.1>
- Wang Q, Wu J, Lei T et al (2014) Temporal-spatial characteristics of severe drought events and their impact on agriculture on a global scale. *Quat Int* 349:10–21. <https://doi.org/10.1016/j.quaint.2014.06.021>
- Wilhite D, Svoboda M, Hayes M (2007) Understanding the complex impacts of drought: A key to enhancing drought mitigation and preparedness. *Water Resour Manag* 21:763–774. <https://doi.org/10.1007/s11269-006-9076-5>
- Xiao L, Chen X, Zhang R, Zhang Z (2019) Spatiotemporal Evolution of Droughts and Their Teleconnections with Large-Scale Climate Indices over Guizhou Province in Southwest China. *Water* 11:2104. <https://doi.org/10.3390/w11102104>
- Xing Y, Shao D, Liang Q et al (2022) Investigation of the drainage loss effects with a street view based drainage calculation method in hydrodynamic modelling of pluvial floods in urbanized area. *J Hydrol* 605:127365. <https://doi.org/10.1016/j.jhydrol.2021.127365>
- Xu Y, Wu X, Kumar R et al (2020) Substantial Increase in the Joint Occurrence and Human Exposure of Heatwave and High-PM Hazards Over South Asia in the Mid-21st Century. *AGU Adv* 1:1–19. <https://doi.org/10.1029/2019AV000103>
- Yang Y, Gan T, Tan X (2020) Spatiotemporal changes of drought characteristics and their dynamic drivers in Canada. *Atmos Res* 232:104695. <https://doi.org/10.1016/j.atmosres.2019.104695>
- Yao N, Li L, Feng P et al (2020) Projections of drought characteristics in China based on a standardized precipitation and evapotranspiration index and multiple GCMs. *Sci Total Environ* 704:135245. <https://doi.org/10.1016/j.scitotenv.2019.135245>
- Yevjevich V (1967) An objective approach to definitions and investigations of continental hydrological droughts. *Hydrol Pap*

- Yin J, Guo S, Wu X et al (2019) A meta-heuristic approach for multivariate design flood quantile estimation incorporating historical information. *Hydrol Res* 50:526–544. <https://doi.org/10.2166/nh.2018.060>
- Zhai J, Mondal S, Fischer T et al (2020) Future drought characteristics through a multi-model ensemble from CMIP6 over South Asia. *Atmos Res* 246:105111. <https://doi.org/10.1016/j.atmosres.2020.105111>
- Zhao C, Brissette F, Chen J, Martel J (2020) Frequency change of future extreme summer meteorological and hydrological droughts over North America. *J Hydrol* 584:124316. <https://doi.org/10.1016/j.jhydrol.2019.124316>
- Zheng Y, He Y, Chen X (2017) Spatiotemporal pattern of precipitation concentration and its possible causes in the Pearl River basin, China. *J Clean Prod* 161:1020–1031. <https://doi.org/10.1016/j.jclepro.2017.06.156>
- Zhao C, Brissette F, Chen J, Martel J (2020) Frequency change of future extreme summer meteorological and hydrological droughts over North America. *J Hydrol* 584:124316. <https://doi.org/10.1016/j.jhydrol.2019.124316>
- Zheng Y, He Y, Chen X (2017) Spatiotemporal pattern of precipitation concentration and its possible causes in the Pearl River basin, China. *J Clean Prod* 161:1020–1031. <https://doi.org/10.1016/j.jclepro.2017.06.156>

Publisher's Note Springer Nature remains neutral with regard to jurisdictional claims in published maps and institutional affiliations.

Springer Nature or its licensor holds exclusive rights to this article under a publishing agreement with the author(s) or other rightsholder(s); author self-archiving of the accepted manuscript version of this article is solely governed by the terms of such publishing agreement and applicable law.

Supplementary Information The online version contains supplementary material available at <https://doi.org/10.1007/s00382-022-06443-6>.